Referee: 2

We reflected all the comments by the reviewer. The criticism and suggestions by the reviewer were appropriate and improved the quality of our manuscript. We appreciate such efforts.

This manuscript describes an OE-based approach to retrieve AOT and SSA using OMI near-UV channels. Conceptually, it is a good idea to take into consideration the inherent measurement/retrieval uncertainties and a priori knowledge; however, it is not convincing that this approach is superior and has the potential to replace the current operational algorithm. My general comments are the followings:

1. This OE-based approach doesn't address the root of the retrieval problems by improving the cloud screening, using more accurate surface reflectance, vertical profile, and aerosol models. It appears that, in terms of retrieval, other than introducing a statistically based cost function, the basics are the same as the operational algorithm. If this new cost function (Eq. 2) is dominated by the difference from the measurement which I assumed the operational algorithm tries to minimize, then it is not surprise that the OE retrievals are not quite different from the operational results. Figures 6 and 7 show the similar results from the operational and OE-based algorithms other than some outliers are eliminated by the latter.

Ans) The near UV aerosol retrieval algorithm has been developed during last few decades through multidirectional efforts. However, improvements of aerosol inversion products using hyperspectral sensors such as OMI and GOME are quite challenging due to the relatively large ground pixel size compared to typical imagers. However, the decadal aerosol information derived using the near UV channel since TOMS is unique, thus valuable, so that it has potential to be used at various field including climatology and air quality. The main purpose of this study is to suggest an alternative inversion method which provides additional information (error estimates, degrees of freedom, cost function, etc.) on the retrievals to optimize the applicability. However, authors agree that the manuscript did not state the purpose of the study clearly as the referee indicated. Several sentences were

inserted/modified to emphasize the advantage of this study. The manuscript was revised as follows:

Following sentences were inserted in the introduction of the revised manuscript at pages 3, lines 9-11:

"The inversion products from such measurements provide various parameters of aerosols at diverse channels. Thus, appropriate sources of aerosol information needs to be employed for relevant studies."

At pages 3 lines 23 – pages 4 lines 29:

"However, deriving information on aerosol using available hyperspectral measurements such as OMI is quite challenging due to the relatively low spatial resolution compared to typical imagers. Thus, the error estimates of retrievals using such sensors are particularly important to understand the reliability of the information, so that it can be used appropriately. The main objective of this study is to improve the applicability of the aerosol inversion products of OMI by providing the reliable error estimates of the retrievals."

At pages 21 lines 444 – lines 449:

"Note that the relative significances of the ε_fs of retrievals depend on their condition. It is additional merit of the error analysis using OE method that it provides specific error estimates of individual target event retrieval (e.g., dust or biomass burning event). While analysis studies using satellite inversion products have often suffered from the statistic reliabilities, more accurate error estimates in this study are expected to contribute to the assessment of the significances of the analysis."

In order to emphasize the advantage of the iterative inversion method, following sentence was inserted in the revised manuscript at pages 4, lines 39-41:

"In addition, iterative inversion methods such as OE provide additional retrieval masking parameters (e.g., cost function and convergence criteria)."

Also, please see the answer of comment 3 for advantage of online inversion method.

2. For the error characterization, the merit of this OE-based approach should be a more

accurate estimation of error for individual retrievals, i.e., the points on Figure 8b should be more or less along the dotted lines. More than 80% of retrievals falling between the dotted lines actually indicate a general overestimation of retrieval errors. It is disappointing that the OE-estimated errors are interpreted as the upper limit (envelope curve) instead of actual retrieval uncertainties; Also the claim of better performance of this error estimation is a little misleading since the error range is actually wider than the operational uncertainty envelope (±30% or 0.1). Based on Figure 8b, the estimated error for AOT of 1.5 is about 0.6 which gives an uncertainty range of about 40% of retrieved AOT.

Ans) Evaluation of the actual radiometric calibration error is still challenging since the calibration methods also have their uncertainties. The 2% of the BSDF error estimation also includes the calibration method and it represents the typical error at whole wavelength domain of OMI (Jaross, 2015, personal communication). For those reasons, the 2% of BSDF uncertainty leads to general overestimates of the error and it is still challenging to evaluate. In our experience, assuming BSDF calibration error as 1% was appropriate at 354 and 388 nm for the retrieval algorithm. Thus, authors regarded the BSDF error as 1% in the revised manuscript. Following sentences were revised in the revised manuscript at pages 11, lines 205-209:

"However, the reported BSDF uncertainty includes the errors in the calibration method and it represents whole wavelength domain. Thus, actual BSDF uncertainty at 354 and 388 nm would be less than 2% (Jaross, 2015). In our experience, 2% of BSDF uncertainty leads to the overestimates of the error and it is still challenging to evaluate. According to multiple retrieval tests, the BSDF uncertainty was assumed to be 1% in this study."

As the measurement error covariance matrix was changed, all retrieval process in the manuscript was re-performed with the latter error covariance matrix, which was reflected throughout the manuscript. The change slightly affects the retrieval values and validation results except the error estimates. The Figure 4-9 was revised in the revised manuscript. The estimated error of the retrieval has been reduced as shown in Figure 5 and 8 as follows:

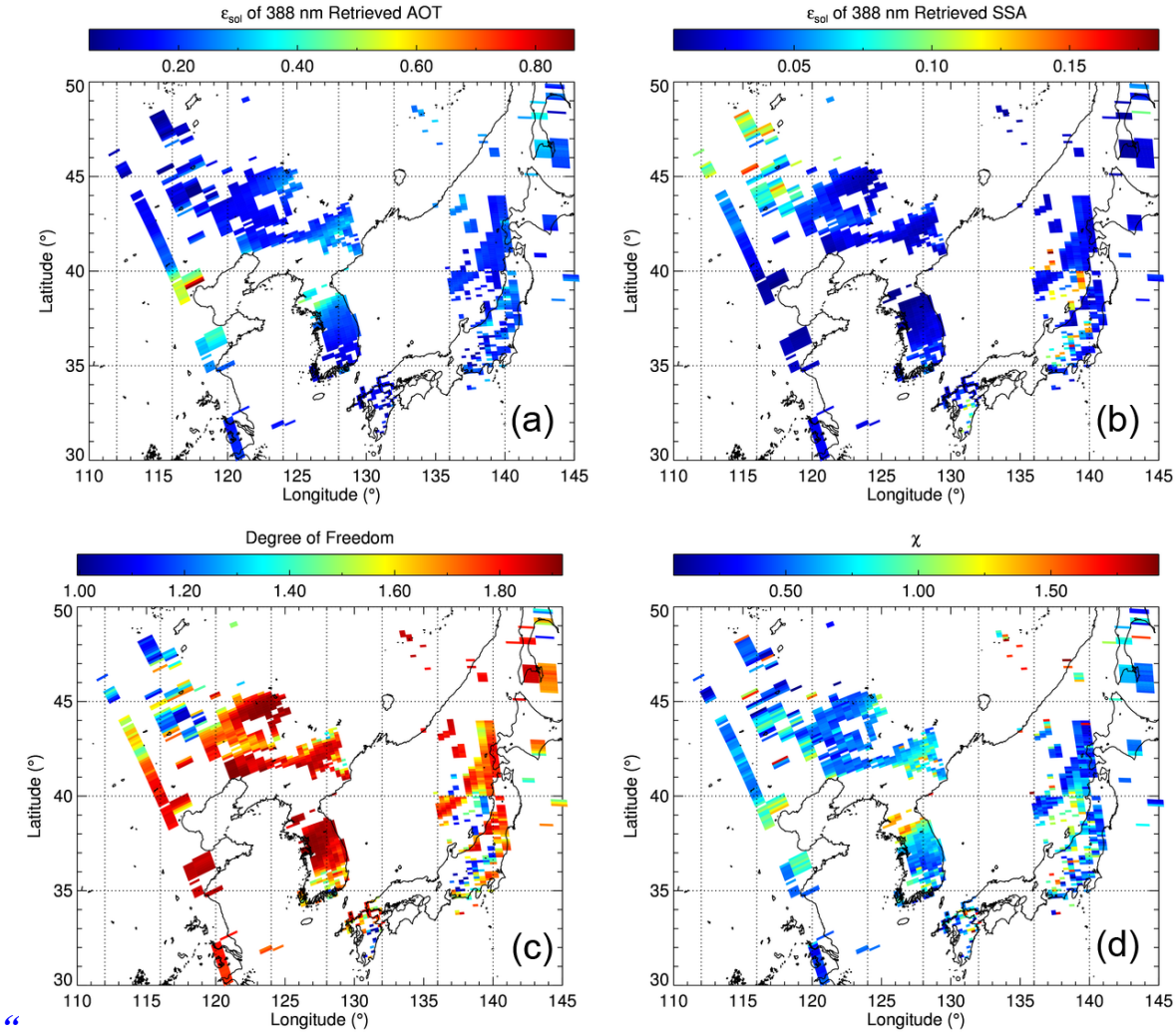

“

Figure 5. *Estimated solution error of (a) OE-based 388 nm AOT and (b) SSA. Panels (c) and (d) show the degrees of freedom and cost function of the retrieval, respectively.*

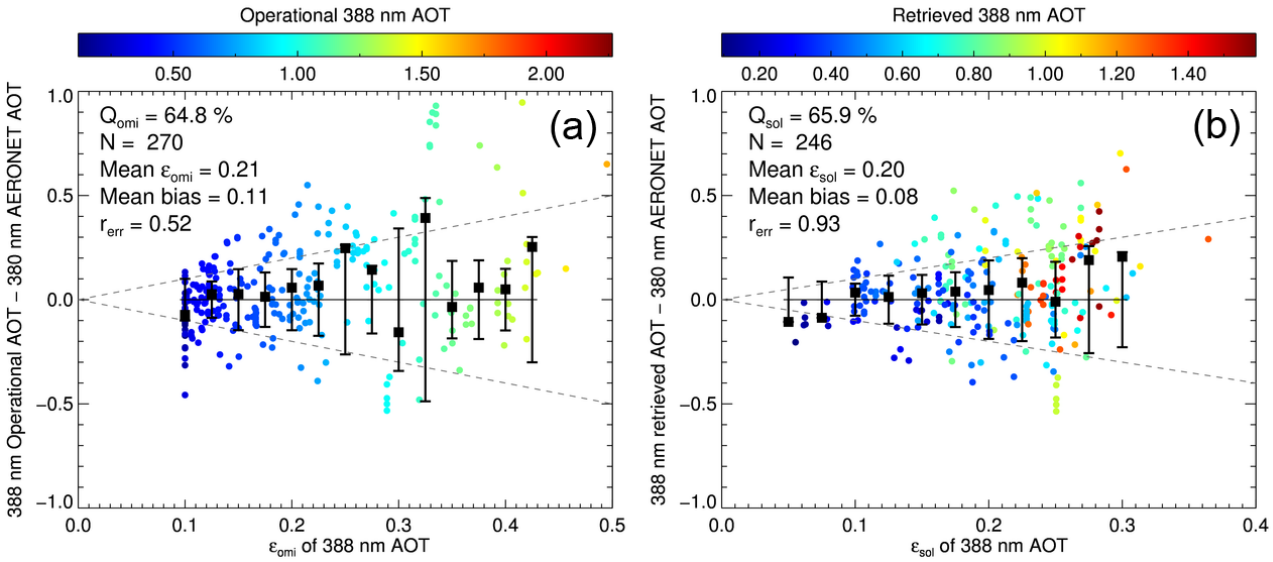

Figure 8. *Comparison between estimated uncertainties of the 388 nm AOT (x-axis) and biases of retrieved AOT from AERONET measurements (y-axis). The panels (a) and (b) are based on the operational and OE-based retrieval/error-estimation algorithm, respectively.*

As shown in Figure 8 (b), the OE-based retrieval error better represents the variances of the actual biases (r=0.93, MB=0.08) than operational error estimation method (Figure 8 (a), r=0.52, MB=0.11). Furthermore, the ratio of error falling within the estimated error of OE method (Q_{sol}= 65.9%) was higher than that of operational method (Q_{omi} = 64.8%), despite that the mean estimated error of OE method (0.20) was lower than that of operational method (0.21). Also, the mean systematic biases from the AERONET was smaller (0.08) than the operational method (0.11) when cost-function cut-off was applied. Following sentences was added in revised manuscript at pages 18-19, lines 370-383 as:

"The estimated retrieval uncertainties of the AOT at 388 nm from the operational algorithm (ε_{omi}, ±30% or 0.1) and estimated ε_{sol} were plotted against the biases relative to AERONET measurements as shown in Figure 8. The percentages of AOT retrieval biases from AERONET falling within the estimated retrieval errors of operational (Q_{omi}) and OE-based method (Q_{sol}) were 64.8% and 65.9%, respectively. The Q_{sol} was higher than Q_{omi} despite of the lower mean value of ε_{sol} (0.20) than that of ε_{omi} (0.21). The error bars and black squares in Figure 8 represent the moving σ and average value of the retrieval biases

from AERONET as a function of estimated error, respectively. As shown in Figure 8 (b), ε_{sol} better explained the moving σ of the actual biases (r=0.93) than ε_{omi} in Figure 8 (a) (r=0.52). Fisher's z-value between the correlation coefficients was 2.33 with two-tailed p-value of 0.02. The systematic biases of ε_{sol} and ε_{omi} (represented by the moving average of each error estimates) are typically related to other error sources, including forward model parameters and sub-pixel cloud contaminations. Since the ε_{sol} of retrieved AOT considers the theoretical sensitivity of the retrieval biases to associated parameters, it explained the retrieval uncertainties better than the ε_{omi}, which only considers the retrieved AOT values."

3. For the online radiative transfer calculations, it is not clear how significant the improvements (eliminate interpolation errors and improve stability) are than using the traditional lookup tables. I hope the authors can have a discussion about the tradeoff between increase of accuracy and loss of efficiency, and whether it is recommended to use this method in operational retrieval.

Ans) We agree that it was not clear how significant the improvements were. However, interpolation error of LUT method typically depends on the interpolation method, resolution of the nodal points, and analytic characteristics of the parameters in LUT, which is hard to evaluate due to such dependency, thus depends on individual algorithm design preference. Therefore, rather than suggesting quantitative significances of the accuracy improvements of the online calculations, more detailed discussions were added in the revised manuscript. Following sentences of discussion about online calculation method were added in the revised manuscript at pages 8-9 at lines 145-165 as:

"Such interpolation error typically depends on the interpolation method, number of the nodal points, and analytic characteristics of the parameters in LUT. In order to reduce the interpolation error, higher resolution of LUT nodal points is necessary which requires larger amount of numerical computation. Furthermore, in order to modify the retrieval algorithm, whole LUT should be re-calculated even for the few number of target retrievals. The errors from the interpolation are also hard to evaluate as the LUT becomes more complicated.

On the contrary, online retrieval methods can reduce such errors from the interpolation and numerically efficient particularly for the smaller number of target retrievals. Thus, online retrieval method is appropriate for the research purposes since retrieval sensitivity study typically use smaller number of sample compared to the operational purposes and prefer rapid and accurate results. In our experience, the online retrieval method was numerically more efficient compared to the LUT-based retrieval method by order of 1 or 2 for less than few thousands of retrievals. Furthermore, the online retrieval methods are optimized to avoid local minima by employing additional constraints to find more reliable and stable solutions (Kalman, 1960;Phillips, 1962;Tikhonov, 1963;Twomey, 1963;Chahine, 1968). However, employing online calculation as operational retrieval method requires large computation cost. Thus, using the online calculation as a benchmark results for the LUT-based algorithm is recommended to develop the optimized LUT for the operational purposes. Recent efforts to minimize the numerical cost of radiative transfer model and to increased calculation speed are expected to make the online calculation more practical even for the operational purposes."

We also concluded that the advantage of this study is to provide more accurate error estimates by OE method as mentioned in general comments #1 rather than the online calculation. In addition, the OE method is one of the online calculation methods. Thus the title of this study was revised as follows:

"An optimal estimation based aerosol retrieval algorithm using OMI near-UV observations"

4. Another general comment is about the comparison between the operational and OE-based retrieval results. Since this manuscript has so much focus on statistics, it is a bit disappointing to see the comparison is not examined in terms of statistical significance, it would be more convincing that "the OE method showed better results" if the difference is statistically significant.

Ans) As the referee suggested, Fisher's z-values and Student's t-values were provided to evaluate the significances of the improvements. Following sentences were revised in the

manuscript at pages 17, lines 340-344:

"The Fisher's z-value between the correlation coefficients (Fisher, 1921) was 3.04 corresponding to two-tailed p-value of 0.0024. The Student's t-value for the difference between the two slopes is 2.10 with 512 degrees of freedom with two-tailed p-value of 0.04. The statistical values show that the difference between two correlation coefficients and slopes are significant (p-value < 0.05)."

And at pages 18, lines 358-366:

"The retrieved 388 nm SSA from both the operational and OE-based algorithms showed similar correlation with the AERONET (r = 0.27 and 0.26 for operational and OE-based algorithms, respectively. Fisher's z-value is 0.1 with two-tailed p-value of 0.92). The retrieved SSA at 388 nm from the operational and OE-based algorithms showed slightly higher correlation with the converted 388 nm SSA from AERONET (r = 0.34 and 0.33 for the operational and OE-based algorithm, respectively) than with the 440 nm SSA from AERONET. However, the significances of the differences in r between converted and unconverted SSA comparisons were low (Fisher's z-values were 0.71 and 0.67 with two-tailed p-values of 0.48 and 0.50 for operational algorithm and OE-based algorithm, respectively)."

My specific comments:

1. Line 65, delete "(2013)"

Ans) Following sentence was modified in the revised manuscript at pages 7, lines 116-117 as:

"The overall concept and design of the improved OMAERUV algorithm is well described by Torres et al. (2013)."

2. Line 119, "and spectral contrast, I354/I388, for the measurement vector"

Ans) Following sentence was modified at revised manuscript at pages 10, lines 190-192 as:

"As described above, the OMI near-UV algorithm uses radiance (I_{388}) and spectral contrast (I_{354}/I_{388}) for the measurement vector, where I_{354} and I_{388} are the normalized radiances at 354 nm and 388 nm, respectively."

3. Line 133-160, in this section, there is confusion about the terms of "uncertainty" and "error" and symbols of σ and ε. For example line 138 says ελ is "the absolute uncertainty" which is the "square root of the sum of squared radiometric random noise and calibration accuracy" (line 133), while Eq. 6 indicates it is the sum of "the random and system components radiometric error" (line 145).

Ans) Sorry for the confusion. As the referee suggested, the definition of the symbols and terminology of error, uncertainty, and accuracy are clarified at the revised manuscript at pages 11, lines 209 – pages 12, lines 222 as follows:

"The radiometric error covariance at each wavelength was calculated from the square root of the sum of squared radiometric uncertainty and calibration accuracy. The error covariance matrix can be written as:

$$\boldsymbol{S}_{\epsilon} = \begin{bmatrix} \sigma(\epsilon_{388})^2 & \sigma(\epsilon_{388}, \epsilon_{354/388})^2 \\ \sigma(\epsilon_{388}, \epsilon_{354/388})^2 & \sigma(\epsilon_{354/388})^2 \end{bmatrix} \quad (5)$$

where ϵ_{λ} is the total error of the measured radiance at wavelength λ, $\epsilon_{354/388}$ is the error of I_{354}/I_{388}, which is described later in this section, and $\sigma(\epsilon_{388}, \epsilon_{354/388})^2$ is the covariance between the total measurement errors of I_{388} and I_{354}/I_{388}.

The ϵ_{λ} typically includes both random and systematic components and its covariance can be expressed as follows:

$$\sigma(\epsilon_\lambda)^2 = \sigma\left(\epsilon_{r,\lambda}\right)^2 + \sigma\left(\epsilon_{s,\lambda}\right)^2 \quad (6)$$

where $\epsilon_{r,\lambda}$ and $\epsilon_{s,\lambda}$ are the random and systematic components of radiometric error at λ, and $\sigma\left(\epsilon_{r,\lambda}\right)^2$ and $\sigma\left(\epsilon_{s,\lambda}\right)^2$ are their covariance values, respectively."

4. Line 211, the references are missing.

Ans) Following references were inserted in the revised manuscript:

"Spurr, R., Wang, J., Zeng, J., and Mishchenko, M. I.: Linearized T-matrix and Mie scattering computations, J Quant Spectrosc Ra, 113, 425-439, 10.1016/j.jqsrt.2011.11.014, 2012.

Spurr, R., and Christi, M.: On the generation of atmospheric property Jacobians from the (V)LIDORT linearized radiative transfer models, J Quant Spectrosc Ra, 142, 109-115, 10.1016/j.jqsrt.2014.03.011, 2014."

An optimal estimation based aerosol retrieval algorithm using OMI near-UV observations

Ukkyo Jeong[1], Jhoon Kim[1,*], Changwoo Ahn[2], Omar Torres[3], Xiong Liu[4], Pawan K. Bhartia[3], Robert J.D. Spurr[5], David Haffner[3], Kelly Chance[4], and Brent N. Holben[3]

[1]Dept. of Atmospheric Sciences, Yonsei University, Seoul, Korea

[2]Science Systems and Applications, Inc., Lanham, Maryland, USA

[3]Goddard Space Flight Center, NASA, Greenbelt, Maryland, USA

[4]Harvard-Smithsonian Center for Astrophysics, Cambridge, Massachusetts, USA

[5]RT Solutions, Inc., 9 Channing Street, Cambridge, Massachusetts, USA

*Corresponding author: Jhoon Kim (jkim2@yonsei.ac.kr)

Tel. +82-2-2123-5682, Fax. +82-2-365-5163

Abstract

An optimal estimation (OE) based aerosol retrieval algorithm using the OMI (Ozone Monitoring Instrument) near-ultraviolet observation was developed in this study. The OE-based algorithm has the merit of providing useful estimates of errors simultaneously with the inversion products. Furthermore, instead of using the traditional look-up tables for inversion, it performs online radiative transfer calculations with the Vector Linearized Discrete Ordinate Radiative Transfer (VLIDORT) model to eliminate interpolation errors and improve stability. The measurements and inversion products of the Distributed Regional Aerosol Gridded Observation Network campaign in Northeast Asia (DRAGON NE-Asia 2012) were used to validate the retrieved AOT and SSA. The retrieved AOT and SSA at 388 nm have a correlation with the Aerosol Robotic Network (AERONET) products that is comparable to or better than the correlation with the operational product during the campaign. The OE-based estimated error better represented the variance of actual biases of AOT at 388 nm between the retrieval and AERONET measurements than the operational error estimates. The forward model parameter errors were analyzed separately for both AOT and SSA retrievals. The surface reflectance at 388 nm, the imaginary part of the refractive index at 354 nm, and the number fine mode fraction (FMF) were found to be the most important parameters affecting the retrieval accuracy of AOT, while FMF was the most important parameter for the SSA retrieval. The additional information provided with the retrievals, including the estimated error and degrees of freedom, is expected to be valuable for relevant studies. Detailed advantages of using the OE method were described and discussed in this paper.

Key words

Aerosol; Error Analysis; Ozone Monitoring Instrument; Optimal Estimation Method; DRAGON

campaign

1. Introduction

Anthropogenic aerosols have affected both the radiative and meteorological balance in the atmosphere and thus the radiative forcing of the atmosphere directly and indirectly (Ramanathan et al., 2001;Russell et al., 1999;Breon et al., 2002). To understand the role of aerosol in the atmosphere from a global perspective, reliable aerosol data from satellites are essential (Al-Saadi et al., 2005;Kinne et al., 2006). The several satellite-based aerosol retrieval methods based on multi-wavelength (Levy et al., 2007;Kim et al., 2007), multi-angle (Fisher et al., 2014), active light (Young et al., 2013), and polarization (Deuze et al., 2001) measurements have their own advantages and limitations. The inversion products from such measurements provide various parameters of aerosols at different channels. Thus, appropriate sources of aerosol information need to be employed for relevant studies.

An important advantage of using the ultraviolet (UV) channel to retrieve aerosol optical properties is that the results are less affected by uncertainties in surface reflectance (Torres et al., 1998). The retrieved aerosol products have relatively uniform quality over both land and ocean except over ice–snow surfaces (Torres et al., 2007;Herman et al., 1997). The near-UV technique for aerosol remote sensing has the additional merit of a long term data record including aerosol absorption properties of over 30 years starting from the launch of the Total Ozone Mapping Spectrometer (TOMS) on Nimbus-7 in 1978 (Torres et al., 1998;Torres et al., 2002a;Torres et al., 2005). Thus, the retrieved products using the near-UV technique from TOMS and Ozone Monitoring Instrument (OMI) measurements are appropriate for climatological research (Torres et al., 2002b;Torres et al., 2007). Information on aerosol extinction and absorption properties in the UV region is also important for estimating the air mass factor (AMF) for trace gas retrievals (Palmer et al., 2001;Lin et al., 2014). However, deriving information on aerosol using available hyperspectral measurements such as OMI and Global Ozone Monitoring Experiment (GOME) is

quite challenging due to the relatively low spatial resolution compared to typical imagers. Thus, the error estimates of retrievals using such sensors are particularly important to understand the reliability of the information, so that it can be used appropriately. The main objective of this study is to improve the applicability of the aerosol inversion products of OMI by providing the reliable error estimates of the retrievals.

Accuracy assessments of the retrieved aerosol optical properties using UV radiances have been performed by comparison with results from reference methods including ground, airborne, and satellite based remote sensing techniques (Torres et al., 2005;Jethva et al., 2014;Torres et al., 2002a;Ahn et al., 2014;Livingston et al., 2009;Ahn et al., 2008;Curier et al., 2008). The aerosol information content of selected OMI spectral radiances using a multi-wavelength algorithm has been estimated using principal component analysis for simulated radiances (Veihelmann et al., 2007). Uncertainty estimates of UV aerosol retrievals have also been calculated by perturbation analysis (Torres et al., 1998;Torres et al., 2002b). Inversion algorithms based on optimal estimation (OE) theory provide not only a constrained solution with respect to the *a priori* information but also detailed error analysis from well-categorized error sources (Rodgers, 2000). In addition, iterative inversion methods such as OE provide additional retrieval masking parameters (*e.g.*, cost function and convergence criteria). Recently developed OE-based retrieval methods have provided both improved inversion products and error estimates from the aerosol and surface error sources (Wagner et al., 2010;Govaerts et al., 2010;Wurl et al., 2010).

A large amount of aerosol is emitted from both natural and anthropogenic sources in East Asia (Lee et al., 2012). The spatial and temporal variations in aerosol optical properties are significant because of the diverse emission sources and trans-boundary transport (Jeong et al., 2011). Thus, the assumed aerosol inversion parameters may cause substantial uncertainties in the retrieval. However, there are insufficient ground-based measurements of aerosol optical properties with

suitable spatial and temporal coverage in East Asia, despite their importance for global air quality and climate change. The Distributed Regional Aerosol Gridded Observation Network Northeast Asia (DRAGON-NE Asia) 2012 campaign (http://aeronet.gsfc.nasa.gov/new_web/DRAGON-Asia_2012_Japan_South_Korea.html) provides valuable datasets including both urban and regional-scale observations at more than 40 sites in Northeast Asia. In the present study, an OE-based near-UV aerosol retrieval and error analysis algorithm is developed to provide both improved aerosol inversion products and estimates of their uncertainties. The retrieved aerosol products and estimated uncertainties are validated against the DRAGON-NE Asia 2012 campaign measurements.

2. Data

OMI is a nadir-viewing hyperspectral spectrometer aboard the EOS (Earth Observing System)-Aura spacecraft that measures upwelling radiances from the top of the atmosphere in the ultraviolet and visible (270–500 nm) regions with approximate spectral resolution of 0.5 nm (Levelt et al., 2006). The advantage of using OMI for aerosol retrieval is its higher spatial resolution than other UV hyperspectral spectrometers (from 13×24 km^2 at nadir to 28×150 km^2 at the swath extremes with median pixel size 15×32 km^2) together with its 2600-km-wide swath. The radiometric calibration procedure and the estimated accuracy of OMI are described in Dobber et al. (2006). To determine aerosol type and vertical distribution, the current OMI near-UV aerosol algorithm (OMAERUV) employs the Cloud–Aerosol Lidar with Orthogonal Polarization (CALIOP) monthly climatology of aerosol layer height and real-time Atmospheric Infrared Sounder (AIRS) carbon monoxide (CO) observations (Torres et al., 2013). Surface reflectances at 354 nm and 388 nm were assumed to be Lambertian and were taken from the TOMS climatology database. Aerosol vertical distribution and surface reflectance information identical to that used in the operational algorithm were used for the OE-based algorithm here.

In this study, the spatial and temporal domains for analysis were confined to the DRAGON-NE Asia 2012 campaign as shown in Figure 1 and Table 1. The gridded observation networks had high spatial resolution over the representative megacities in Northeast Asia: Seoul in South Korea and Osaka in Japan. To validate and compare the retrieved aerosol products from OMI, level 2 campaign products were used from the aerosol robotic network (AERONET); 380 nm aerosol optical thickness (AOT) from direct sun measurements and spectral single scattering albedo (SSA) from almucantar inversion products (Holben et al., 1998;Dubovik and King, 2000;Dubovik et al., 2000;Dubovik et al., 2006). Retrieved 388 nm AOT from OMI was validated against AERONET 380 nm AOT. The OMI AOT retrievals within a radius of 0.5° of the AERONET site and within ±30 minutes of the OMI overpass time (about 13:40 local time) were averaged. The resulting OMI AOT average values were then compared with the time-averaged Sun photometer measurements.

Aerosol absorption properties are retrieved at different wavelengths by AERONET and OMI. The AERONET inversion products of the SSA are available at 440, 670, 860, and 1020 nm, while the OMAERUV algorithm retrieves the SSA at 354 nm and 388 nm. Earlier field studies found that aerosol absorption is a continuous function of wavelength in the ultraviolet to short infrared region (Kirchstetter et al., 2004;Russell et al., 2010). To compare the SSA values from OMI and AERONET at the same wavelength, the AERONET SSA at 388 nm was obtained by extrapolating the SSAs at 440–1020 nm using a spline function. Then the converted AERONET SSA at 388 nm was compared with the retrieved OMI SSA values even though uncertainties might exist in the transformation. Unlike the direct sun measurements including AOT, the inversion products of AERONET from almucantar measurements are retrieved less frequently and require appropriate atmospheric conditions for AOT (440 nm AOT > 0.4) and solar zenith angle (solar zenith angle > 45°) (Dubovik and King, 2000;Jethva et al., 2014). Such favorable atmospheric

conditions for the inversion using almucantar measurements rarely overlap closely with the OMI overpass time. Furthermore, too narrow a time window around the satellite overpass time reduces the number of comparison samples. In this study, to secure enough data points the SSA of a region at OMI overpass time was assumed to adequately represent the daily values. For the comparison, the converted 388 nm SSA from AERONET was averaged over a day and the OMI retrievals of 388 nm SSA were spatially averaged over a grid area of 0.5° × 0.5° centered on the AERONET site.

3. Method

3.1. Operational OMI near UV aerosol algorithm

The OMAERUV uses two channel radiances at 354 nm and 388 nm to estimate aerosol amount and absorption properties (Torres et al., 1998;Torres et al., 2007;Torres et al., 2013). AOT and SSA at 388 nm are retrieved from pre-calculated reflectance look-up tables (LUT) for pre-determined nodal points of observational geometry and aerosol optical properties, total optical depth, and aerosol layer height. Three major aerosol types are considered and listed in Table 2: desert dust, carbonaceous aerosols associated with biomass burning, and weakly absorbing sulfate-based aerosols (hereafter dust, smoke, and sulfate, respectively). Each aerosol type has an assumed particle size distribution (PSD) derived from the long-term statistics of AERONET inversion products. The UV real refractive index (n_r) is obtained from the Optical Properties Of Aerosols And Clouds (OPAC) database (Hess et al., 1998). In the operational algorithm, the imaginary refractive indices (n_i) at 354 nm are assumed to be 1.0, 1.2, and 1.4 times the retrieved n_i at 388 nm for sulfate, smoke, and dust aerosol, respectively (Torres et al., 2007;Jethva and Torres, 2011). The overall concept and design of the improved OMAERUV algorithm is well described by Torres et al. (2013).

There have been further improvements at updated OMAERUV (version 1.5.3), which was

used for reprocessing the data of AOT and SSA in this study. The OMAERUV algorithm was refined by adjusting thresholds of UV aerosol index (UVAI) and Atmospheric Infrared Sounder (AIRS) CO data in determining aerosol types and retrieval approaches. A cloud screening scheme in assigning algorithm quality flags was also modified for retaining more good retrievals of carbonaceous and sulfate type aerosols when the CO level is high enough (higher than 3.2×10^{18} molecules·cm^{-2}) with various reflectivity thresholds. The UVAI threshold was changed from 0.8 to 0.5 over the oceans. This modification eliminates the land-ocean discontinuity in UVAI threshold. It is now identical (0.5) for both conditions. The current characterization of ocean reflective properties in the OMAERUV algorithm does not explicitly account for ocean color effects and, therefore, the quality of the retrieved aerosol properties over the oceans for low aerosol amounts would be highly uncertain. For that reason, retrievals over the oceans are only carried out for high concentrations of either desert dust or carbonaceous aerosols as indicated by UVAI values larger than or equal to 0.5.

Depending on the magnitude of the UVAI and CO parameters as well as the aerosol type, two retrieval approaches are currently used. They are referred to as two-channel and single-channel retrievals. In the two-channel approach, observations at 354 and 388 nm are used to simultaneously derive AOD and SSA. Over scenes when the aerosol absorption signal is low, the single-channel retrieval is applied. AOD is retrieved from the 388 nm observation assuming a value of 1.0 for SSA. Different CO threshold values are used for the northern and southern hemispheres to remove upper tropospheric CO which may not be necessarily associated with carbonaceous aerosols. A smoothing function in CO is used to transition from SH to NH threshold values. Specific criteria for retrieval approaches are summarized in Table 3. More detailed information of the latest update in OMAERUV is available from the Readme file at the web site (http://disc.sci.gsfc.nasa.gov/Aura/data-holdings/OMI/omaeruv_v003.shtml).

3.2. OE-based OMI near UV aerosol algorithm

The traditional LUT-based inversion method potentially includes errors due to interpolation between the nodal points and the local minimum, despite its high numerical efficiency. Such interpolation error typically depends on the interpolation method, number of the nodal points, and analytic characteristics of the parameters in LUT. In order to reduce the interpolation error, higher resolution of LUT nodal points is necessary which requires larger amount of numerical computation. Furthermore, in order to modify the retrieval algorithm, whole LUT should be re-calculated even for a few number of target retrievals. The errors from the interpolation are also hard to evaluate as the LUT becomes more complicated.

On the contrary, online retrieval methods can reduce such errors from the interpolation and are numerically efficient particularly for the smaller number of target retrievals. Thus, online retrieval method is appropriate for the research purposes since retrieval sensitivity study typically use smaller number of sample compared to the operational purposes and prefer rapid and accurate results. In our experience, the online retrieval method was numerically more efficient compared to the LUT-based retrieval method by order of 1 or 2 for less than few thousands of retrievals. Furthermore, the online retrieval methods are optimized to avoid local minima by employing additional constraints to find more reliable and stable solutions (Kalman, 1960;Phillips, 1962;Tikhonov, 1963;Twomey, 1963;Chahine, 1968). However, employing online calculation as operational retrieval method requires large computation cost. Thus, using the online calculation as a benchmark results for the LUT-based algorithm is recommended to develop the optimized LUT for the operational purposes. Recent efforts to minimize the numerical cost of radiative transfer model and to increased calculation speed are expected to make the online calculation more practical even for the operational purposes.

Optimization for measurement error, the inclusion of *a priori* and ancillary data, and

168 employing physical constraints (*e.g.,* non-negativity of measurements and retrievals) for an
169 inversion method are important since each method has its own advantages and disadvantages
170 (Dubovik, 2004). In this study, we used OE as the inversion method (Rodgers, 2000) since it has
171 several advantages over other methods for OMI-like measurements, as discussed in Section 4. The
172 atmospheric inverse problem often suffers from both insufficient information content of the
173 measurements and imperfect measurement accuracy. Bayesian statistics provides mapping methods
174 from the measurement probability density function (pdf) into state space with prior knowledge.
175 Based on Bayes' theorem, the OE technique employs additional constraints from external sources (*a*
176 *priori*) to complement the insufficient information content of the measurements. For the nonlinear
177 inversion case, by considering the maximum *a posteriori* approach, the general form of the
178 Bayesian solution can be expressed as Equation (1) where measurement and *a priori* errors are
179 assumed to be Gaussian (Rodgers, 2000):

180

181 $$-2\ln P(\mathbf{x}|\mathbf{y}) = [\mathbf{y}-\mathbf{K}\mathbf{x}]^T\mathbf{S}_\epsilon^{-1}[\mathbf{y}-\mathbf{K}\mathbf{x}] + [\mathbf{x}-\mathbf{x}_a]^T\mathbf{S}_a^{-1}[\mathbf{x}-\mathbf{x}_a] + \mathbf{c} \quad (1)$$

182

183 where $\mathbf{x}$ is the state vector and $\mathbf{y}$ the measurement vector, $\mathbf{K}$ is the weighting function matrix,
184 $\mathbf{S}_\epsilon$ is the measurement error covariance matrix, $\mathbf{x}_a$ is the *a priori* mean state, and $\mathbf{S}_a$ is the *a*
185 *priori* covariance matrix. The formulation finds the optimized solution that minimizes the cost
186 function (χ):

187

$$\chi^2 = \left\|\mathbf{S}_\epsilon^{-\frac{1}{2}}(\mathbf{y}-\mathbf{K}\mathbf{x})\right\|_2^2 + \left\|\mathbf{S}_a^{-\frac{1}{2}}(\mathbf{x}-\mathbf{x}_a)\right\|_2^2 \quad (2)$$

Detailed derivations and implications are described in previous studies (Rodgers, 2000;Wurl et al., 2010;Govaerts et al., 2010). As described above, the OMI near-UV algorithm uses radiance (I_{388}) and spectral contrast (I_{354}/I_{388}) for the measurement vector, where I_{354} and I_{388} are the normalized radiances at 354 nm and 388 nm, respectively. The state vector in this study is the AOT at 388 nm (τ_{388}) and the imaginary refractive index at 388 nm ($n_{i,388}$). Then, the weighting function matrix can be expressed as follows:

$$\mathbf{K} = \begin{bmatrix} \frac{\partial I_{388}}{\partial \tau_{388}} & \frac{\partial I_{388}}{\partial n_{i,388}} \\ \frac{\partial}{\partial \tau_{388}}\left(\frac{I_{354}}{I_{388}}\right) & \frac{\partial}{\partial n_{i,388}}\left(\frac{I_{354}}{I_{388}}\right) \end{bmatrix} \quad (3)$$

where the weighting function of the spectral contrast can be obtained from the following derivative:

$$\frac{\partial}{\partial x}\left(\frac{I_{354}}{I_{388}}\right) = \frac{\frac{\partial I_{354}}{\partial x} I_{388} - I_{354} \frac{\partial I_{388}}{\partial x}}{(I_{388})^2} \quad (4)$$

In typical inversion methods, including OE, estimation of the reliable measurement error covariance matrix is important to determine the likelihood of the solution (Govaerts et al., 2010). The measurement error includes radiometric noise error and calibration accuracy. The absolute bidirectional scattering distribution function (BSDF) radiometric accuracy of the OMI instrument is reported to be about 4% for 2σ and the random noise error is provided in the level 1b product

(Dobber et al., 2006). However, the reported BSDF uncertainty includes the errors in the calibration method and it represents whole wavelength domain. Thus, actual BSDF uncertainty at 354 and 388 nm would be less than 2% (Jaross, 2015). In our experience, 2% of BSDF uncertainty leads to the overestimates of the error and it is still challenging to evaluate. According to multiple retrieval tests, the BSDF uncertainty was assumed to be 1% in this study. The radiometric error covariance at each wavelength was calculated from the square root of the sum of squared radiometric uncertainty and calibration accuracy. The error covariance matrix can be written as:

$$\mathbf{S}_{\epsilon} = \begin{bmatrix} \sigma(\epsilon_{388})^2 & \sigma\left(\epsilon_{388}, \epsilon_{354/388}\right)^2 \\ \sigma\left(\epsilon_{388}, \epsilon_{354/388}\right)^2 & \sigma\left(\epsilon_{354/388}\right)^2 \end{bmatrix} \quad (5)$$

where ϵ_{λ} is the total error of the measured radiance at wavelength λ, $\epsilon_{354/388}$ is the error of I_{354}/I_{388}, which is described later in this section, and $\sigma\left(\epsilon_{388}, \epsilon_{354/388}\right)^2$ is the covariance between the total measurement errors of I_{388} and I_{354}/I_{388}.

The ϵ_{λ} typically includes both random and systematic components and its covariance can be expressed as follows:

$$\sigma(\epsilon_{\lambda})^2 = \sigma\left(\epsilon_{r,\lambda}\right)^2 + \sigma\left(\epsilon_{s,\lambda}\right)^2 \quad (6)$$

where $\epsilon_{r,\lambda}$ and $\epsilon_{s,\lambda}$ are the random and systematic components of radiometric error at λ, and $\sigma(\epsilon_{r,\lambda})^2$ and $\sigma(\epsilon_{s,\lambda})^2$ are their covariance values, respectively. The $\epsilon_{354/388}$ can be approximated as follows:

$$\epsilon_{354/388} \cong \frac{I_{354}}{I_{388}} - \frac{I_{354}+\epsilon_{354}}{I_{388}+\epsilon_{388}} \cong \frac{I_{354}}{I_{388}}\left(\frac{\epsilon_{354}}{I_{354}} - \frac{\epsilon_{388}}{I_{388}}\right) \cong \frac{I_{354}}{I_{388}}\left(\frac{\epsilon_{s,354}}{I_{354}} - \frac{\epsilon_{s,388}}{I_{388}} + \frac{\epsilon_{\mathrm{r},354}}{I_{354}} - \frac{\epsilon_{\mathrm{r},388}}{I_{388}}\right) \quad (7)$$

When the systematic components of the measurement errors of radiances at 354 nm and 388 nm are positively correlated and their values are similar, part of the systematic uncertainties can be reduced by the $\frac{\epsilon_{s,354}}{I_{354}} - \frac{\epsilon_{s,388}}{I_{388}}$ term. However, assessment of the systematic error of OMI measurements at each pixel is still challenging despite this partial reduction of systematic errors by using I_{354}/I_{388}. In this study, the BSDF calibration uncertainties of I_{354} and I_{388} at a pixel are assumed to be systematic and similar, while the radiometric noise values of I_{354} and I_{388} are assumed to be random and independent. Then, the systematic measurement error of $\epsilon_{354/388}$ can be regarded as negligible and the covariance of $\epsilon_{354/388}$ in Equation (7) can be approximated as follows:

$$\sigma(\epsilon_{354/388}) \cong \frac{I_{354}}{I_{388}}\sqrt{\left(\frac{\epsilon_{\mathrm{r},354}}{I_{354}}\right)^2 + \left(\frac{\epsilon_{\mathrm{r},388}}{I_{388}}\right)^2} \quad (8)$$

The $\sigma(\epsilon_{388}, \epsilon_{354/388})^2$ can be obtained as follows:

$$\sigma\left(\epsilon_{388}, \epsilon_{354/388}\right)^2 = \frac{1}{n-1}\sum_{i=1}^{n} {\epsilon_{388}}^i {\epsilon_{354/388}}^i \quad (9)$$

238

239 where ${\epsilon_{388}}^i$ and ${\epsilon_{354/388}}^i$ are the uncertainties in the i^{th} measurement of I_{388} and I_{354}/I_{388} for
240 a sample of size *n*, respectively. Under the same assumptions used in Equations (7) and (8),
241 ${\epsilon_{354/388}}^i$ has only random and independent components, and so $\sigma\left(\epsilon_{388}, \epsilon_{354/388}\right)$ can be regarded
242 as negligible. The diagonal and off-diagonal elements of the measurement error covariance matrices
243 using two different measurement matrices are compared in Table 4.

244

245 **3.3. Error characterization**

246 Retrieved products with estimated and/or characterized error are valuable for any
247 application. Various error sources can be categorized as shown in the following equation by
248 linearizing the forward model with respect to associated parameters (Eyre, 1987;Rodgers, 1990,
249 2000):

250

$$\hat{\mathbf{x}} - \mathbf{x} = (\mathbf{A} - \mathbf{I}_n)(\mathbf{x} - \mathbf{x}_a) + \mathbf{G}_y\mathbf{K}_b\left(\mathbf{b} - \hat{\mathbf{b}}\right) + \mathbf{G}_y\Delta\mathbf{f}\left(\mathbf{x}, \mathbf{b}, \mathbf{b}'\right) + \mathbf{G}_y\boldsymbol{\epsilon} \quad (10)$$

251

252 where $\hat{\mathbf{x}}$ and $\mathbf{x}$ are the retrieval and true states, respectively; $\mathbf{A}$ is the averaging kernel matrix; $\mathbf{I}_n$
253 is the identity matrix; $\mathbf{x}_a$ is the *a priori* state vector; $\mathbf{G}_y$ is the contribution function matrix; $\mathbf{K}_b$
254 is the weighting function matrix of forward model parameters ($\mathbf{b}$); $\hat{\mathbf{b}}$ is the guessed forward model

parameter; $\Delta\mathbf{f}$ is the error in the forward model relative to the real physics; and $\boldsymbol{\epsilon}$ is the measurement error. The first and last term on the right-hand-side (RHS) of Equation (10) is the smoothing error and retrieval noise, respectively. Their covariance matrices can be calculated from:

$$\mathbf{S}_s = (\mathbf{A} - \mathbf{I}_n)\mathbf{S}_E(\mathbf{A} - \mathbf{I}_n)^{\mathrm{T}} \tag{11}$$

$$\mathbf{S}_n = \mathbf{G}_y\mathbf{S}_{\boldsymbol{\epsilon}}{\mathbf{G}_y}^{\mathrm{T}} \tag{12}$$

where $\mathbf{S}_s$ is the smoothing error covariance matrix, $\mathbf{S}_E$ is the covariance of the ensemble of states about the mean state, and $\mathbf{S}_n$ is the covariance matrix of the retrieval noise. We have assumed that the climatological value is a good representation of the real ensemble of the state about the mean state, and so the covariance matrix of the *a priori* state was employed as the $\mathbf{S}_E$ in this study. Each $\mathbf{S}_s$ and $\mathbf{S}_n$ has two diagonal elements that represent the variances of the smoothing error and retrieval noise for two retrievals, AOT and SSA. The smoothing error (ε_{sm}) and retrieval noise (ε_n) of AOT and SSA were defined as the square root of the corresponding diagonal elements of $\mathbf{S}_s$ and $\mathbf{S}_n$, respectively. The square root of the sum of squared ε_{sm} and ε_n of AOT and SSA are defined in this study as the solution errors (ε_{sol}) of AOT and SSA, respectively.

The second term on the RHS of Equation (10) is the forward model parameter error, and its covariance matrix can be calculated as follows:

$$\mathbf{S}_f = \mathbf{G}_y\mathbf{K}_b\mathbf{S}_b{\mathbf{K}_b}^{\mathrm{T}}{\mathbf{G}_y}^{\mathrm{T}} \tag{13}$$

where $\mathbf{S}_f$ is the covariance matrix of the forward model parameter error, and $\mathbf{S}_b$ is the error covariance matrix of forward model parameter, $\mathbf{b}$. The forward model parameters of the near-UV method include the aerosol microphysical model parameters, aerosol vertical distribution, meteorological profile (pressure and temperature), and surface properties. These forward model parameters contain both random and systematic components with different scales of spatial and temporal variation. Furthermore, each forward model parameter has a different uncertainty that is difficult to evaluate. In this study, $\mathbf{S}_f$ was analyzed separately with respect to each forward model parameter as suggested by Rodgers (2000). The forward model parameter error (ε_f) of AOT and SSA were obtained from the square root of the corresponding diagonal elements of each $\mathbf{S}_f$.

The third term on the RHS in Equation (10) is the forward model error that is caused by discrepancies between known and real physics. To simulate the earth-reflected radiance, VLIDORT (linearized pseudo-spherical vector discrete ordinate radiative transfer code, version 2.6) was used. This code is based on one of the most accurate radiative transfer solutions for a one-dimensional atmosphere (Spurr, 2006). Linearization of state vectors and forward model parameters are described in prior papers (Spurr et al., 2012;Spurr and Christi, 2014). Although the simulated radiances are expected to be accurate, the forward model error depends on factors including the number of streams, layers, and Legendre coefficients for the aerosol phase functions. To reduce the numerical errors that can arise from an insufficient number of coefficients, 3 Stokes parameters, 75 layers, 16 streams, and up to 500 Legendre coefficients for the aerosol phase matrix were used for the radiance simulations. However, it is still a challenge to evaluate other possible sources of forward model error such as Raman scattering and the three-dimensional effect of the atmosphere for retrieval. Such issues are beyond the scope of this study, and thus only smoothing error, retrieval noise, and forward model parameter error are evaluated here.

3.4. *A priori* characterization

Using reliable *a priori* information is important in the OE method since the final solutions are determined between the *a priori* state and the inversion space of a measurement. There are several sources of *a priori* information including climatological data, reliable measurements from more accurate instruments, and calculations from models based on theoretical or empirical statistics (Govaerts et al., 2010;Wurl et al., 2010;Rodgers, 2000). Appropriate sources of *a priori* depend on the characteristics of the state vector and the accuracy of the *a priori* database. When the *a priori* state has a systematic bias away from the true state, this bias propagates to the retrieval products. In this study, 10 years (from 2005 to 2014) of OMAERUV 388 nm AOT and SSA in spring (from March to May) were used for the *a priori* data. Figure 2 shows the collected climatological data of the 388 nm AOT and SSA in East Asia used in this study. To avoid biases due to cloud contamination in the OMI products, averaged values and standard deviations (σ) with more than 70 data points were used.

4. Results

The dust event on 28th April 2012 has been selected to compare the aerosol optical properties from the operational product with the OE-based retrievals in this study. Figure 3 shows the true color image on that day from the Moderate Resolution Imaging Spectroradiometer (MODIS) Aqua and the UV aerosol index from OMI. To see the difference between the OE-based and operational algorithm in the same area, both methods were applied to measurements with an operational algorithm flag of 0, to avoid cloud contamination and radiometric calibration uncertainties. Some of the points retrieved by the operational algorithm were rejected in the OE-based retrievals when the cost function cut-off was applied, as described in this section.

320 The AOT and SSA at 388 nm from the operational and OE-based products are compared in
321 Figure 4. The ε_{sol} of the retrieved AOT and SSA at 388 nm, degree of freedom, and χ are shown
322 in Figure 5. The OE-based and operational AOT at 388 nm are similar, as shown in Figure 4 (a) and
323 (b). Both products seem to be affected by snow and cloud contaminated pixels around Seoul in
324 South Korea (37°N, 126°E), Tianjin in China (39°N, 116°E) and Nagano in Japan (36°N, 138°E).
325 In Figure 5 (a), the ε_{sol} of retrieved AOT at 388 nm has relatively high values compared with the
326 AOT level at large viewing zenith angle. Noticeable discrepancies of SSA at 388 nm from the
327 operational and OE-based products are evident in some of the areas as shown in Figure 4 (c) and (d).
328 The operational algorithm performed single-channel retrieval around East Mongolia (47°N, 115°E),
329 while the OE-based algorithm performed two-channel retrieval for all cases. Since this area has a
330 low level of AOT, the information content of aerosol absorption property is insufficient, resulting in
331 the low degrees of freedom shown in Figure 4 (b) and Figure 5 (c). Thus the OE-based SSA in this
332 area (Figure 4 (d)) seems noisy and the ε_{sol} of SSA appears high. Similar results for the behavior
333 of SSA are apparent around central Japan (38°N, 138°E). Thus, SSA values with high AOT and low
334 ε_{sol} are recommended for the analysis, similar to the retrieval conditions for AERONET inversion
335 products (Dubovik and King, 2000). Additional information provided on retrievals at each pixel in
336 Figure 5 is expected to be valuable for relevant studies including trace gas retrieval and data
337 assimilation.

338 Figure 6 shows the results of validation of operational and OE-based AOT retrievals at 388
339 nm. As shown in Figure 6 (a) and (b), the OE-based inversion method showed higher correlation
340 coefficient (r = 0.82) and slightly improved slope (0.83) and offset (0.16) values than the
341 operational algorithm (r = 0.71, slope = 0.71, and offset = 0.2). The Fisher's z-value between the
342 correlation coefficients (Fisher, 1921) was 3.04 corresponding to two-tailed p-value of 0.0024. The
343 Student's t-value for the difference between the two slopes is 2.10 with 512 degrees of freedom with

the two-tailed p-value of 0.04. The statistical values show that difference between the two correlation coefficients and slopes are significant (p-value < 0.05). The Q values (percentage of AOT retrievals falling within an uncertainty envelope of ±30% or 0.1) of the OE-based retrievals and operational algorithm were similar (63.0%). When a measured radiance is affected by parameters that the theoretical radiative transfer model does not consider (*e.g.*, sub-pixel cloud contamination), the χ of the retrieval typically has a high value. In this study, retrievals with χ larger than a certain value (*i.e.*, 2.0 in this study) have been rejected. This limitation on retrievals imposed by the χ reduced the number of retrievals with abnormally high biases, which might be associated with sub-pixel cloud contamination, in the operational algorithm in Figure 6 (a).

The SSA values at 388 nm from OMI operational products and OE-based inversion products were compared with those at 388 nm and 440 nm from AERONET inversion products as shown in Figure 7. The retrieved SSA at 388 nm from the operational algorithm showed comparable or higher values of $Q_{0.03}$ (59.2%) and $Q_{0.05}$ (85.1%) with those from the OE-based algorithm ($Q_{0.03}$ = 53.5%, $Q_{0.05}$ = 86.0%) when compared with the AERONET SSA at 440 nm (The $Q_{0.03}$ and $Q_{0.05}$ represent the percentage of SSA retrievals falling within an uncertainty envelope of ±0.03 and ±0.05, respectively). The retrieved 388 nm SSA from both the operational and OE-based algorithms showed similar correlation with the AERONET (r = 0.27 and 0.26 for operational and OE-based algorithms, respectively. Fisher's z-value is 0.1 with two-tailed p-value of 0.92). The retrieved SSA at 388 nm from the operational and OE-based algorithms showed slightly higher correlation with the converted 388 nm SSA from AERONET (r = 0.34 and 0.33 for the operational and OE-based algorithm, respectively) than with the 440 nm SSA from AERONET. However, the significances of the differences in r between converted and unconverted SSA comparisons were low (Fisher's z-values were 0.71 and 0.67 with two-tailed p-values of 0.48 and 0.50 for operational algorithm and OE-based algorithm, respectively). The retrieved SSA at 388 nm from the

operational algorithm also showed comparable or higher values of $Q_{0.03}$ (59.2%) and $Q_{0.05}$ (83.9%) than those of the OE-based algorithm ($Q_{0.03}$ = 53.5%, $Q_{0.05}$ = 82.8%) when compared with converted SSA at 388 nm from AERONET.

The estimated retrieval uncertainties of the AOT at 388 nm from the operational algorithm (ε_{omi}, ±30% or 0.1) and estimated ε_{sol} were plotted against the biases relative to AERONET measurements as shown in Figure 8. The percentages of AOT retrieval biases from AERONET falling within the estimated retrieval errors of operational (Q_{omi}) and OE-based method (Q_{sol}) were 64.8% and 65.9%, respectively. The Q_{sol} was higher than Q_{omi} despite of the lower mean value of ε_{sol} (0.20) than that of ε_{omi} (0.21). The error bars and black squares in Figure 8 represent the moving σ and average value of the retrieval biases from AERONET as a function of estimated error, respectively. As shown in Figure 8 (b), ε_{sol} better explained the moving σ of the actual biases (r=0.93) than ε_{omi} in Figure 8 (a) (r=0.52). Fisher's z-value between the correlation coefficients was 2.33 with two-tailed p-value of 0.02. The systematic biases of ε_{sol} and ε_{omi} (represented by the moving average of each error estimates) are typically related to other error sources, including forward model parameters and sub-pixel cloud contaminations. Since the ε_{sol} of retrieved AOT considers the theoretical sensitivity of the retrieval biases to associated parameters, it explained the retrieval uncertainties better than the ε_{omi}, which only considers the retrieved AOT values.

Table 5 shows the suggested error sources and their magnitudes from the OMI ATBD (Algorithm Theoretical Basis Documents) (Torres et al., 2002b) and the values employed in this study. Although the current OMI cloud masking method is based on long-term TOMS heritage, there may still be ground pixels contaminated by sub-pixel clouds. As the TOA reflectance is greatly increased by even a small amount of cloud, cloud contamination can cause large positive biases in the AOT retrieval. Previous studies estimated the AOT retrieval errors due to 5% cloud contamination to be of the order of 0.1 to 0.2 (Torres et al., 1998;Torres et al., 2002b). They also

reported an even higher error in the single scattering albedo (0 to 0.15) especially for strongly absorbing aerosols. However, estimation of sub-pixel cloud contamination is difficult because of the large spatio-temporal variability of clouds and the relatively large ground pixel size of OMI. Thus the further error analysis of cloud contamination error budget from Torres et al. (2002b) was not performed in this study. Typical uncertainties of the 354 nm and 388 nm surface reflectances were assumed to be 0.01 for both land and ocean. The BSDF accuracy was assumed to be 1% (Dobber et al., 2006;Jaross, 2015), and radiometric precision from OMI Level 1b data. To analyze the uncertainty associated with the aerosol size information and refractive index, σ values of the size parameter and n_r at 440 nm were taken from AERONET inversion products during the campaign period. To analyze the assumed n_i at 354 nm, the $\mathbf{S}_b$ was also obtained from AERONET statistics during the campaign period. Aerosol vertical distribution is important as it affects aerosol retrieval using near-UV and blue channels, particularly for absorbing aerosols (Torres et al., 1998;de Graaf et al., 2005;Torres et al., 2013). However, accuracy assessments of the aerosol height information used are still challenging. Typical uncertainties of the assumed aerosol layer peak height and half width were assumed to be 2 km and 1 km, respectively, in this study. In the OE-based near-UV aerosol retrieval algorithm, all aerosols are assumed to be spherical and the optical properties are calculated from aerosol microphysical properties using the Mie solution. However, non-sphericity may cause significant uncertainties, especially for large particles (Mishchenko and Travis, 1994;Mishchenko et al., 1995;Mishchenko et al., 1997;Mishchenko et al., 2003;Dubovik et al., 2006), and aerosol morphology is quite complicated and requires further analysis for the near-UV region. This is out of the scope of this study and thus needs to be investigated in a future study. Therefore the uncertainties due to aerosol non-sphericity were not analyzed.

Figure 9 shows the average and σ values of ε_f of the retrieved AOT and SSA that were sampled for the validation in Figure 6 (b) and Figure 7 (b), (d). High values of ε_f for AOT

appeared in n_i at 354 nm (0.34±0.25), surface reflectance at 388 nm (0.19±0.07), and the number fine mode fraction (FMF) (0.16±0.09). These values are higher or comparable with the mean ε_{sol} of retrieved AOT at 388 nm (0.20). Thus, the accuracy of AOT retrievals depends on not only the radiometric accuracy and information content but also the aerosol models and ancillary data of the surface reflectance, of which the effect is already well known. The FMFs of the sulfate (0.999596) and smoke type aerosols (0.999795) are similar while that for dust type aerosols is quite different (0.995650). Considering that the estimated σ value for FMF uncertainty in this study (0.0015, see Table 5) is much lower than the difference between the FMFs of dust type and other aerosols (~0.004, see Table 2), the errors resulting from selection of the wrong aerosol type can be more significant. The estimated ε_f of the surface reflectance at 388 nm was higher than the previously suggested value (0.07–0.09 for AOT and <0.01 for SSA) in the OMI ATBD (Torres et al., 2002b). The ε_fs of AOT with respect to the surface reflectance at 354 nm (0.12±0.04), peak height of the aerosol vertical distribution (0.11±0.10), fine mode n_r (0.09±0.10), half width of the fine mode PSD (0.07±0.06), mean radius of the coarse mode PSD (0.06±0.03), and half width of the aerosol vertical distribution (0.06±0.05) showed similar moderate sensitivity. Those for the mean radius of the fine mode PSD (0.02±0.02) and half width of the coarse mode PSD (0.02±0.01) were smaller and that of the coarse mode n_r (0.003±0.004) was found to be negligible.

Among ε_fs of the SSA retrieval, the FMF error ($1.4\times10^{-2} \pm 6.4\times10^{-3}$) was the most important of the ε_fs of the SSA retrieval. Errors in n_i at 354 nm ($7.4\times10^{-3} \pm 2.8\times10^{-3}$) and the peak height of the aerosol vertical distribution ($5.2\times10^{-3} \pm 2.8\times10^{-3}$) were found to be the second most important. The ε_f of SSA with respect to the fine mode n_r ($3.9\times10^{-3} \pm 1.7\times10^{-3}$), width of the fine mode PSD ($3.8\times10^{-3} \pm 1.7\times10^{-3}$), the surface reflectance at 354 nm ($3.4\times10^{-3} \pm 1.8\times10^{-3}$) and 388 nm ($2.8\times10^{-3} \pm 2.1\times10^{-1}$), mean radius of the coarse mode PSD ($3.1\times10^{-3} \pm 1.1\times10^{-3}$), half width of the aerosol vertical distribution ($2.3\times10^{-3} \pm 1.5\times10^{-3}$), mean radius of the fine mode PSD

440 ($1.1\times10^{-3} \pm 5.7\times10^{-4}$) and width of the coarse mode PSD ($8.7\times10^{-4} \pm 3.3\times10^{-4}$) were smaller and
441 that of the coarse mode n_r ($5.2\times10^{-5} \pm 1.3\times10^{-4}$) appeared to be negligible. The estimated ε_fs of
442 SSA were found to be about a factor magnitude lower than the ε_{sol} of SSA. The mean values of
443 ε_{sm} and ε_n of SSA were 0.023 and 0.029, respectively. Thus, the estimated ε_{sol} of SSA at 388
444 nm is expected to be more reliable and represent the total uncertainties of SSA, since the
445 uncertainty in SSA is predominantly affected by ε_{sol}, while uncertainty in AOT is affected by both
446 ε_{sol} and ε_f. Note that the relative significances of the ε_fs of retrievals depend on their condition.
447 It is additional merit of the error analysis using OE method that it provides specific error estimates
448 of individual target event retrieval (*e.g.,* dust or biomass burning event). While analysis studies
449 using satellite inversion products have often suffered from the statistic reliabilities, more reliable
450 error estimates in this study are expected to contribute to the assessment of significances of the
451 analysis.

452

453 **5. Summary and Discussion**

454 An OE-based aerosol retrieval and error characterization algorithm using the OMI near-UV
455 radiances was developed in this study. The climatological values of OMAERUV products were
456 employed as *a priori* data for the inversion method. The OE-based inversion method developed
457 here provides not only the retrieved values of AOT and SSA but also estimates of their uncertainties.
458 The retrieved AOT and SSA at 388 nm were compared with the AERONET products during the
459 DRAGON-NE Asia 2012 campaign. The retrieved AOT using the OE method showed better results
460 than the operational product. The OE-based SSA at 388 nm showed consistency with AERONET
461 inversion products comparable to that of the operational SSA. The estimated retrieval noise and
462 smoothing error of OE-based AOT represented well the variances of actual biases between the
463 retrieved AOT and AERONET AOT. The forward model parameter errors were analyzed separately

for both AOT and SSA inversion products. Uncertainties of surface reflectance at 388 nm, imaginary refractive index at 354 nm and number fine mode fraction were found to be the most important parameters affecting the retrieval accuracy of AOT, while uncertainties in the coarse mode real part of the refractive index had negligible effect. For SSA retrieval accuracy, number fine mode fraction was found to be the most important parameter while the other parameters appeared to have relatively small effects. As the FMF depends on the aerosol type, it is expected that more accurate aerosol type classification might improve the retrieval accuracy of AOT and SSA. For AOT retrieval, the estimated ε_f was comparable with the ε_{sol}, while the ε_f of SSA was negligible compared to the ε_{sol} of the retrieved SSA. It is also found that a sufficient amount of aerosol loading is necessary for reliable SSA retrieval.

However, there are still error sources which need to be analyzed, including the *a priori* error from climatology, aerosol morphology, cloud contamination, and three dimensional effects of radiative transfer. The assumed conditions in the inversion procedure also differ from the real state. Validation studies for a longer period at more types of site are also necessary. Securing a more reliable *a priori* database is expected to improve the OE-based aerosol retrieval algorithm.

Acknowledgements

This research was supported by the GEMS program of the Ministry of Environment, Korea and the Eco Innovation Program of KEITI (2012000160002). The authors also acknowledge the KNMI and NASA/GSFC for providing OMI and AERONET data.

485 **References**

486 Ahn, C., Torres, O., and Bhartia, P. K.: Comparison of ozone monitoring instrument UV aerosol
487 products with Aqua/Moderate Resolution Imaging Spectroradiometer and Multiangle Imaging
488 Spectroradiometer observations in 2006, J Geophys Res-Atmos, 113, Artn D16s27 Doi
489 10.1029/2007jd008832, 2008.

490 Ahn, C., Torres, O., and Jethva, H.: Assessment of OMI near-UV aerosol optical depth over land, J
491 Geophys Res-Atmos, 119, 2457-2473, Doi 10.1002/2013jd020188, 2014.

492 Al-Saadi, J., Szykman, J., Pierce, R. B., Kittaka, C., Neil, D., Chu, D. A., Remer, L., Gumley, L.,
493 Prins, E., Weinstock, L., MacDonald, C., Wayland, R., Dimmick, F., and Fishman, J.:
494 Improving national air quality forecasts with satellite aerosol observations, B Am Meteorol
495 Soc, 86, 1249-+, Doi 10.1175/Bams-86-9-1249, 2005.

496 Breon, F. M., Tanre, D., and Generoso, S.: Aerosol effect on cloud droplet size monitored from
497 satellite, Science, 295, 834-838, DOI 10.1126/science.1066434, 2002.

498 Chahine, M. T.: Determination of temperature profile in an atmosphere from its outgoing radiance,
499 J. Opt. Soc. Am., 12, 1634-1637, 1968.

500 Curier, R. L., Veefkind, J. P., Braak, R., Veihelmann, B., Torres, O., and de Leeuw, G.: Retrieval of
501 aerosol optical properties from OMI radiances using a multiwavelength algorithm: Application
502 to western Europe, J Geophys Res-Atmos, 113, Artn D17s90 Doi 10.1029/2007jd008738,
503 2008.

504 de Graaf, M., Stammes, P., Torres, O., and Koelemeijer, R. B. A.: Absorbing Aerosol Index:
505 Sensitivity analysis, application to GOME and comparison with TOMS, J Geophys Res-Atmos,
506 110, Artn D01201 Doi 10.1029/2004jd005178, 2005.

507 Deuze, J. L., Breon, F. M., Devaux, C., Goloub, P., Herman, M., Lafrance, B., Maignan, F.,
508 Marchand, A., Nadal, F., Perry, G., and Tanre, D.: Remote sensing of aerosols over land
509 surfaces from POLDER-ADEOS-1 polarized measurements, J Geophys Res-Atmos, 106,
510 4913-4926, Doi 10.1029/2000jd900364, 2001.

511 Dobber, M. R., Dirksen, R. J., Levelt, P. F., Van den Oord, G. H. J., Voors, R. H. M., Kleipool, Q.,
512 Jaross, G., Kowalewski, M., Hilsenrath, E., Leppelmeier, G. W., de Vries, J., Dierssen, W.,
513 and Rozemeijer, N. C.: Ozone-Monitoring Instrument calibration, Ieee T Geosci Remote, 44,
514 1209-1238, Doi 10.1109/Tgrs.2006.869987, 2006.

515 Dubovik, O., and King, M. D.: A flexible inversion algorithm for retrieval of aerosol optical
516 properties from Sun and sky radiance measurements, J Geophys Res-Atmos, 105, 20673-
517 20696, Doi 10.1029/2000jd900282, 2000.

518 Dubovik, O., Smirnov, A., Holben, B. N., King, M. D., Kaufman, Y. J., Eck, T. F., and Slutsker, I.:
519 Accuracy assessments of aerosol optical properties retrieved from Aerosol Robotic Network
520 (AERONET) Sun and sky radiance measurements, J Geophys Res-Atmos, 105, 9791-9806,
521 Doi 10.1029/2000jd900040, 2000.

522 Dubovik, O.: Optimization of numerical inversion in photopolarimetic remote sensing,
523 Photopolarimetry in Remote Sensing, 65-106, 2004.

524 Dubovik, O., Sinyuk, A., Lapyonok, T., Holben, B. N., Mishchenko, M., Yang, P., Eck, T. F.,
525 Volten, H., Munoz, O., Veihelmann, B., van der Zande, W. J., Leon, J. F., Sorokin, M., and
526 Slutsker, I.: Application of spheroid models to account for aerosol particle nonsphericity in
527 remote sensing of desert dust, J Geophys Res-Atmos, 111, Artn D11208 Doi
528 10.1029/2005jd006619, 2006.

529 Eyre, J. R.: On Systematic-Errors in Satellite Sounding Products and Their Climatological Mean-
530 Values, Q J Roy Meteor Soc, 113, 279-292, Doi 10.1256/Smsqj.47515, 1987.

531 Fisher: On the "probable error" of a coefficient of correlation deduced from a small sample, Metron,
532 1, 3-32, 1921.

533 Fisher, D., Muller, J. P., and Yershov, V. N.: Automated Stereo Retrieval of Smoke Plume Injection
534 Heights and Retrieval of Smoke Plume Masks From AATSR and Their Assessment With
535 CALIPSO and MISR, Ieee T Geosci Remote, 52, 1249-1258, Doi 10.1109/Tgrs.2013.2249073,
536 2014.

537 Govaerts, Y. M., Wagner, S., Lattanzio, A., and Watts, P.: Joint retrieval of surface reflectance and
538 aerosol optical depth from MSG/SEVIRI observations with an optimal estimation approach: 1.
539 Theory, J Geophys Res-Atmos, 115, Artn D02203 Doi 10.1029/2009jd011779, 2010.

540 Herman, J. R., Bhartia, P. K., Torres, O., Hsu, C., Seftor, C., and Celarier, E.: Global distribution of
541 UV-absorbing aerosols from Nimbus 7/TOMS data, J Geophys Res-Atmos, 102, 16911-16922,
542 Doi 10.1029/96jd03680, 1997.

543 Hess, M., Koepke, P., and Schult, I.: Optical properties of aerosols and clouds: The software
544 package OPAC, B Am Meteorol Soc, 79, 831-844, Doi 10.1175/1520-
545 0477(1998)079<0831:Opoaac>2.0.Co;2, 1998.

546 Holben, B. N., Eck, T. F., Slutsker, I., Tanre, D., Buis, J. P., Setzer, A., Vermote, E., Reagan, J. A.,
547 Kaufman, Y. J., Nakajima, T., Lavenu, F., Jankowiak, I., and Smirnov, A.: AERONET - A
548 federated instrument network and data archive for aerosol characterization, Remote Sens
549 Environ, 66, 1-16, Doi 10.1016/S0034-4257(98)00031-5, 1998.

550 Jaross, G.: disccusion of OMI BSDF calibration accuracy, in, edited by: Jeong, U., SSAI, Lanham,

551 Maryland, USA, 2015.

552 Jeong, U., Kim, J., Lee, H., Jung, J., Kim, Y. J., Song, C. H., and Koo, J. H.: Estimation of the
553 contributions of long range transported aerosol in East Asia to carbonaceous aerosol and PM
554 concentrations in Seoul, Korea using highly time resolved measurements: a PSCF model
555 approach, J Environ Monitor, 13, 1905-1918, Doi 10.1039/C0em00659a, 2011.

556 Jethva, H., and Torres, O.: Satellite-based evidence of wavelength-dependent aerosol absorption in
557 biomass burning smoke inferred from Ozone Monitoring Instrument, Atmos Chem Phys, 11,
558 10541-10551, DOI 10.5194/acp-11-10541-2011, 2011.

559 Jethva, H., Torres, O., and Ahn, C.: Global assessment of OMI aerosol single-scattering albedo
560 using ground-based AERONET inversion, J Geophys Res-Atmos, 119, 9020-9040, Doi
561 10.1002/2014jd021672, 2014.

562 Kalman, R. E.: A new approach to linear filtering and prediction problems, Journal of Basic
563 Engineering, 82, 35-45, 1960.

564 Kim, J., Lee, J., Lee, H. C., Higurashi, A., Takemura, T., and Song, C. H.: Consistency of the
565 aerosol type classification from satellite remote sensing during the Atmospheric Brown Cloud-
566 East Asia Regional Experiment campaign, J Geophys Res-Atmos, 112, Artn D22s33 Doi
567 10.1029/2006jd008201, 2007.

568 Kinne, S., Schulz, M., Textor, C., Guibert, S., Balkanski, Y., Bauer, S. E., Berntsen, T., Berglen, T.
569 F., Boucher, O., Chin, M., Collins, W., Dentener, F., Diehl, T., Easter, R., Feichter, J.,
570 Fillmore, D., Ghan, S., Ginoux, P., Gong, S., Grini, A., Hendricks, J. E., Herzog, M., Horowitz,
571 L., Isaksen, I., Iversen, T., Kirkavag, A., Kloster, S., Koch, D., Kristjansson, J. E., Krol, M.,
572 Lauer, A., Lamarque, J. F., Lesins, G., Liu, X., Lohmann, U., Montanaro, V., Myhre, G.,

573 Penner, J. E., Pitari, G., Reddy, S., Seland, O., Stier, P., Takemura, T., and Tie, X.: An
574 AeroCom initial assessment - optical properties in aerosol component modules of global
575 models, Atmos Chem Phys, 6, 1815-1834, 2006.

576 Kirchstetter, T. W., Novakov, T., and Hobbs, P. V.: Evidence that the spectral dependence of light
577 absorption by aerosols is affected by organic carbon, J Geophys Res-Atmos, 109, Artn D21208
578 Doi 10.1029/2004jd004999, 2004.

579 Lee, J., Kim, J., Yang, P., and Hsu, N. C.: Improvement of aerosol optical depth retrieval from
580 MODIS spectral reflectance over the global ocean using new aerosol models archived from
581 AERONET inversion data and tri-axial ellipsoidal dust database, Atmos Chem Phys, 12, 7087-
582 7102, DOI 10.5194/acp-12-7087-2012, 2012.

583 Levelt, P. F., Van den Oord, G. H. J., Dobber, M. R., Malkki, A., Visser, H., de Vries, J., Stammes,
584 P., Lundell, J. O. V., and Saari, H.: The Ozone Monitoring Instrument, Ieee T Geosci Remote,
585 44, 1093-1101, Doi 10.1109/Tgrs.2006.872333, 2006.

586 Levy, R. C., Remer, L. A., Mattoo, S., Vermote, E. F., and Kaufman, Y. J.: Second-generation
587 operational algorithm: Retrieval of aerosol properties over land from inversion of Moderate
588 Resolution Imaging Spectroradiometer spectral reflectance, J Geophys Res-Atmos, 112, Artn
589 D13211 Doi 10.1029/2006jd007811, 2007.

590 Lin, J. T., Martin, R. V., Boersma, K. F., Sneep, M., Stammes, P., Spurr, R., Wang, P., Van
591 Roozendael, M., Clemer, K., and Irie, H.: Retrieving tropospheric nitrogen dioxide from the
592 Ozone Monitoring Instrument: effects of aerosols, surface reflectance anisotropy, and vertical
593 profile of nitrogen dioxide, Atmos Chem Phys, 14, 1441-1461, DOI 10.5194/acp-14-1441-
594 2014, 2014.

595 Livingston, J. M., Redemann, J., Russell, P. B., Torres, O., Veihelmann, B., Veefkind, P., Braak, R.,
596 Smirnov, A., Remer, L., Bergstrom, R. W., Coddington, O., Schmidt, K. S., Pilewskie, P.,
597 Johnson, R., and Zhang, Q.: Comparison of aerosol optical depths from the Ozone Monitoring
598 Instrument (OMI) on Aura with results from airborne sunphotometry, other space and ground
599 measurements during MILAGRO/INTEX-B, Atmos Chem Phys, 9, 6743-6765, 2009.

600 Mishchenko, M. I., and Travis, L. D.: T-Matrix Computations of Light-Scattering by Large
601 Spheroidal Particles, Opt Commun, 109, 16-21, Doi 10.1016/0030-4018(94)90731-5, 1994.

602 Mishchenko, M. I., Lacis, A. A., Carlson, B. E., and Travis, L. D.: Nonsphericity of Dust-Like
603 Tropospheric Aerosols - Implications for Aerosol Remote-Sensing and Climate Modeling,
604 Geophys Res Lett, 22, 1077-1080, Doi 10.1029/95gl00798, 1995.

605 Mishchenko, M. I., Travis, L. D., Kahn, R. A., and West, R. A.: Modeling phase functions for
606 dustlike tropospheric aerosols using a shape mixture of randomly oriented polydisperse
607 spheroids, J Geophys Res-Atmos, 102, 16831-16847, Doi 10.1029/96jd02110, 1997.

608 Mishchenko, M. I., Geogdzhayev, I. V., Liu, L., Ogren, J. A., Lacis, A. A., Rossow, W. B.,
609 Hovenier, J. W., Volten, H., and Munoz, O.: Aerosol retrievals from AVHRR radiances:
610 effects of particle nonsphericity and absorption and an updated long-term global climatology
611 of aerosol properties, J Quant Spectrosc Ra, 79, 953-972, Doi 10.1016/S0022-4073(02)00331-
612 X, 2003.

613 Palmer, P. I., Jacob, D. J., Chance, K., Martin, R. V., Spurr, R. J. D., Kurosu, T. P., Bey, I.,
614 Yantosca, R., Fiore, A., and Li, Q. B.: Air mass factor formulation for spectroscopic
615 measurements from satellites: Application to formaldehyde retrievals from the Global Ozone
616 Monitoring Experiment, J Geophys Res-Atmos, 106, 14539-14550, Doi
617 10.1029/2000jd900772, 2001.

Phillips, B. L.: A technique for numerical solution of certain intergral equation of first kind, Journal of Assoc. Comput. Mach., 9, 84-97, 1962.

Ramanathan, V., Crutzen, P. J., Kiehl, J. T., and Rosenfeld, D.: Atmosphere - Aerosols, climate, and the hydrological cycle, Science, 294, 2119-2124, DOI 10.1126/science.1064034, 2001.

Rodgers, C. D.: Characterization and Error Analysis of Profiles Retrieved from Remote Sounding Measurements, J Geophys Res-Atmos, 95, 5587-5595, Doi 10.1029/Jd095id05p05587, 1990.

Rodgers, C. D.: Inverse method for atmospheric sounding: theory and practice, World Scientific Publishing Co. Pte. Ltd., Singapore, 2000.

Russell, P. B., Hobbs, P. V., and Stowe, L. L.: Aerosol properties and radiative effects in the United States East Coast haze plume: An overview of the Tropospheric Aerosol Radiative Forcing Observational Experiment (TARFOX), J Geophys Res-Atmos, 104, 2213-2222, Doi 10.1029/1998jd200028, 1999.

Russell, P. B., Bergstrom, R. W., Shinozuka, Y., Clarke, A. D., DeCarlo, P. F., Jimenez, J. L., Livingston, J. M., Redemann, J., Dubovik, O., and Strawa, A.: Absorption Angstrom Exponent in AERONET and related data as an indicator of aerosol composition, Atmos Chem Phys, 10, 1155-1169, 2010.

Spurr, R., Wang, J., Zeng, J., and Mishchenko, M. I.: Linearized T-matrix and Mie scattering computations, J Quant Spectrosc Ra, 113, 425-439, 10.1016/j.jqsrt.2011.11.014, 2012.

Spurr, R., and Christi, M.: On the generation of atmospheric property Jacobians from the (V)LIDORT linearized radiative transfer models, J Quant Spectrosc Ra, 142, 109-115, 10.1016/j.jqsrt.2014.03.011, 2014.

Spurr, R. J. D.: VLIDORT: A linearized pseudo-spherical vector discrete ordinate radiative transfer

640 code for forward model and retrieval studies in multilayer multiple scattering media, J Quant
641 Spectrosc Ra, 102, 316-342, DOI 10.1016/j.jqsrt.2006.05.005, 2006.

642 Tikhonov, A. N.: On the solution of incorrectly stated problems and a method of regularization,
643 Dokl. Akad. Nauk., 151, 501-504, 1963.

644 Torres, O., Bhartia, P. K., Herman, J. R., Ahmad, Z., and Gleason, J.: Derivation of aerosol
645 properties from satellite measurements of backscattered ultraviolet radiation: Theoretical basis
646 (vol 103, pg 17099, 1998), J Geophys Res-Atmos, 103, 23321-23321, 1998.

647 Torres, O., Bhartia, P. K., Herman, J. R., Sinyuk, A., Ginoux, P., and Holben, B.: A long-term
648 record of aerosol optical depth from TOMS observations and comparison to AERONET
649 measurements, J Atmos Sci, 59, 398-413, Doi 10.1175/1520-
650 0469(2002)059<0398:Altroa>2.0.Co;2, 2002a.

651 Torres, O., Decae, R., Veefkind, J. P., and de Leeuw, G.: OMI aerosol retrieval algorithm, in OMI
652 Algorithm Theoretical Basis Document, NASA Goddard Space Flight Cent., Greenbelt, Md.,
653 USA, 47-71, 2002b.

654 Torres, O., Bhartia, P. K., Sinyuk, A., Welton, E. J., and Holben, B.: Total Ozone Mapping
655 Spectrometer measurements of aerosol absorption from space: Comparison to SAFARI 2000
656 ground-based observations, J Geophys Res-Atmos, 110, Artn D10s18 Doi 10.1029/Jd004611,
657 2005.

658 Torres, O., Tanskanen, A., Veihelmann, B., Ahn, C., Braak, R., Bhartia, P. K., Veefkind, P., and
659 Levelt, P.: Aerosols and surface UV products from Ozone Monitoring Instrument observations:
660 An overview, J Geophys Res-Atmos, 112, Artn D24s47 Doi 10.1029/2007jd008809, 2007.

661 Torres, O., Ahn, C., and Chen, Z.: Improvements to the OMI near-UV aerosol algorithm using A-

662 train CALIOP and AIRS observations, Atmos Meas Tech, 6, 3257-3270, DOI 10.5194/amt-6-
663 3257-2013, 2013.

664 Twomey, S.: On the numerical solution of Fredholm integral equations of the first kind by the
665 inversion of the linear system produced by quadrature, Journal of Assoc. Comput. Mach., 10,
666 97-101, 1963.

667 Veihelmann, B., Levelt, P. F., Stammes, P., and Veefkind, J. P.: Simulation study of the aerosol
668 information content in OMI spectral reflectance measurements, Atmos Chem Phys, 7, 3115-
669 3127, 2007.

670 Wagner, S. C., Govaerts, Y. M., and Lattanzio, A.: Joint retrieval of surface reflectance and aerosol
671 optical depth from MSG/SEVIRI observations with an optimal estimation approach: 2.
672 Implementation and evaluation, J Geophys Res-Atmos, 115, Artn D02204 Doi
673 10.1029/2009jd011780, 2010.

674 Wurl, D., Grainger, R. G., McDonald, A. J., and Deshler, T.: Optimal estimation retrieval of aerosol
675 microphysical properties from SAGE II satellite observations in the volcanically unperturbed
676 lower stratosphere, Atmos Chem Phys, 10, 4295-4317, DOI 10.5194/acp-10-4295-2010, 2010.

677 Young, S. A., Vaughan, M. A., Kuehn, R. E., and Winker, D. M.: The Retrieval of Profiles of
678 Particulate Extinction from Cloud-Aerosol Lidar and Infrared Pathfinder Satellite Observations
679 (CALIPSO) Data: Uncertainty and Error Sensitivity Analyses, J Atmos Ocean Tech, 30, 395-
680 428, Doi 10.1175/Jtech-D-12-00046.1, 2013.

681

682 **Tables and Figures**

683 **Table captions**

684 **Table 1.** Positions and mean AOT and SSA at 388 nm of the AERONET sites during the
685 DRAGON-NE Asia 2012 campaign.

686 **Table 2.** Aerosol number-size distribution parameters* and real refractive index (n_r) for each
687 aerosol type in the OMI near-UV algorithm.

688 **Table 3.** Retrieval approach criteria of OMI near-UV algorithm version 1.5.3.

689 **Table 4.** Diagonal and off-diagonal elements of the measurement error covariance matrices using
690 two different measurement matrices.

691 **Table 5.** Error sources and their assumed magnitudes in the OMI ATBD (Algorithm Theoretical
692 Basis Documents) and this study.

693

694

List of tables

Table 1. Positions and mean AOT and SSA at 388 nm of the AERONET sites during the DRAGON-NE Asia 2012 campaign.

Site name	Latitude (°) (North)	Longitude (°) (East)	Mean 380 nm AOT	Mean 440 nm SSA
Baengnyeong	37.97	124.63	0.56	0.96
Yonsei Univ., Seoul	37.56	126.94	0.63	0.93
Anmyeon	36.54	126.33	0.57	0.94
Bokjeong, Seoul	37.46	127.13	0.75	0.90
Gangneung Wonju National Univ.	37.77	128.87	0.53	0.92
Guwol, Seoul	37.45	126.72	0.69	0.94
GIST, Gwangju	35.23	126.84	0.54	0.93
HUFS, Yongin	37.34	127.27	0.63	0.90
Kongju National Univ., Kongju	36.47	127.14	0.62	0.96
Konkuk Univ., Seoul	37.54	127.08	0.67	0.92
Korea Univ., Seoul	37.59	127.03	0.73	0.92
Kunsan National Univ., Kunsan	35.94	126.68	0.61	0.92
Kyungil Univ., Kyungsan	36.07	128.82	0.57	0.93
Mokpo National Univ., Mokpo	34.91	126.44	0.58	0.93
NIER, Incheon	37.57	126.64	0.62	0.93
Pusan National Univ., Pusan	35.24	129.08	0.62	0.93
Sanggye, Seoul	37.66	127.07	0.73	0.92

Sinjeong, Seoul	37.52	126.86	0.64	0.91
Soha, Seoul	37.45	126.89	0.69	0.91
Gosan, Jeju	33.29	126.16	0.62	0.96
Seoul National Univ., Seoul	37.46	126.95	0.65	0.93
Fukuoka	33.52	130.48	0.50	0.90
Kohriyama	37.36	140.38	0.34	0.95
Kyoto	35.03	135.78	0.47	0.94
Matsue	35.48	133.01	0.56	0.93
Mt. Ikoma	34.68	135.68	0.39	0.96
Mt. Rokko	34.76	135.23	0.41	0.95
Nara	34.69	135.83	0.48	0.94
Nishiharima	35.03	134.34	0.42	0.95
North Osaka	34.77	135.51	0.52	0.94
South Osaka	34.54	135.50	0.55	0.94
Tsukuba	36.05	140.12	0.38	0.94
Noto	37.33	137.14	0.41	0.94
Shirahama	33.69	135.36	0.41	0.96
Chiba University	35.63	140.10	0.31	0.92
Fukue	32.75	128.68	0.78	0.92

698

699

700

701

Table 2. Aerosol number-size distribution parameters* and real refractive index (n_r) for each aerosol type in the OMI near-UV algorithm.

Aerosol Model	r_g m1 [μm]	r_g m2 [μm]	σ m1 [μm]	σ m2 [μm]	FMF	n_r	$n_{i,354/388}$
Sulfate	0.088	0.509	1.499	2.160	0.999596	1.40	1.0
Smoke	0.080	0.705	1.492	2.075	0.999795	1.50	1.2
Dust	0.052	0.670	1.697	1.806	0.995650	1.55	1.4

*Number-weighted particle size distribution parameters: fine and coarse mode radii (r_g m1 and r_g m2) and variance (σ m1 and σ m2), number fine mode fraction (FMF).

Table 3. Retrieval approach criteria of OMI near-UV algorithm version 1.5.3.

Surface Category	UVAI	CO (10^{18} molecules-cm^{-2})	Surface Type	Aerosol Type	Retrieval Approach
Ocean	≥ 0.5	> 2.2 NH (1.8 SH)	N/A*	Smoke	Two-channel
Ocean	≥ 0.5	≤ 2.2 NH (1.8 SH)	N/A	Dust	Two-channel
Ocean	< 0.5	-	-	-	No retrieval
Land	≥ 0.5	> 2.2 NH (1.8 SH)	All	Smoke	Two-channel
Land	≥ 0.5	≤ 2.2 NH (1.8 SH)	All	Dust	Two-channel
Land	< 0.5	>2.2 NH (1.8 SH)	All	Sulfate	Two-channel
Land	< 0.5	≤ 2.2 NH (1.8 SH)	All but arid	Sulfate	Single channel
Land	< 0.5	≤ 2.2 NH (1.8 SH)	arid	Dust	Single Channel

*Not available.

712 **Table 4.** Diagonal and off-diagonal elements of the measurement error covariance matrices using
713 two different measurement matrices.

Measurement matrix	$[I_{354}\ \ I_{388}]^T$	$\left[I_{354}\ \ \frac{I_{354}}{I_{388}}\right]^T$
First diagonal term	$\sigma(\epsilon_{354})^2$	$\sigma(\epsilon_{388})^2$
Second diagonal term	$\sigma(\epsilon_{388})^2$	$\left(\frac{I_{354}}{I_{388}}\right)^2\left\{\left(\frac{\epsilon_{r,354}}{I_{354}}\right)^2+\left(\frac{\epsilon_{r,388}}{I_{388}}\right)^2\right\}$
Off-diagonal term	$\sigma(\epsilon_{354},\epsilon_{388})^2$	0

714

715 **Table 5.** Error sources and their assumed magnitudes in the OMI ATBD (Algorithm Theoretical
716 Basis Documents) and this study.

Error source	Error perturbation (OMI ATBD)	Assumed value of σ for each error source in this study
Cloud Contamination	5% cloud contamination	NA[+]
Surface Reflectivity	0.01 error in surface reflectivity	0.01 for both wavelengths
Radiometric uncertainty	SNR less than 1% Radiometric offset additive error of 1% Radiometric scale factor multiplicative error of 1%	1% of BSDF calibration uncertainty (Dobber et al., 2006; Jaross, 2015) Radiometric precision provided by Level 1b data
Size distribution (mode radius)	5% increase of mode radius	0.019 for fine mode[*] 0.510 for coarse mode[*]
Size distribution (width)	5% increase of width	0.265 for fine mode[*] 0.307 for coarse mode[*]
Fine mode fraction	NA	0.0015[*]
Refractive index	Increase with 0.05 for n_r Increase with 0.01 for n_i	0.053 for n_r (for all wavelengths and size modes)[*] 0.0047 for 354 nm n_i[*]
Aerosol Vertical Profile	Change of 1 km peak height	Change of 2 km peak height Change of 1 km half width
Particle shape	NA	NA

717 [*]Standard deviation of each parameter during the DRAGON-NE Asia 2012 campaign. The

718 parameters for n_r and n_i were obtained from 440 nm AERONET inversion products.

719 [+]Not analyzed.

720 **Figure captions**

721 **Figure 1.** Mean 380 nm aerosol optical thickness (AOT) and 440 nm single scattering albedo and
722 their probability density functions during the DRAGON-NE Asia 2012 campaign.

723 **Figure 2.** (a) Mean and (b) standard deviation of 388 nm AOT from the OMAERUV product in
724 spring (March to May) 2005–2014. Panels (c) and (d) show the average and standard deviation of
725 SSA, respectively, during the same period.

726 **Figure 3.** (a) MODIS Aqua true color image and (b) UV aerosol index from the OMI product in
727 Northeast Asia on 28th April 2012.

728 **Figure 4.** (a) OMI operational AOT, (b) OE-based AOT, (c) operational SSA, and (d) OE-based
729 SSA on 28th April 2012 at 388 nm.

730 **Figure 5.** Estimated S_{sn} of (a) OE-based 388 nm AOT and (b) SSA. Panels (c) and (d) show the
731 degrees of freedom and cost function of the retrieval, respectively.

732 **Figure 6.** Validation of 388 nm AOT against AERONET data from (a) operational products and (b)
733 the OE-based algorithm during the DRAGON-NE Asia 2012 campaign.

734 **Figure 7.** Comparison of the 440 nm SSA from AERONET and 388 nm SSA from (a) the
735 operational products and (b) the OE-based algorithm, during the DRAGON-NE Asia 2012
736 campaign. Panels (c) and (d) compare converted 388 nm SSA from AERONET with that from (c)
737 the operational products and (d) the OE-based algorithm.

738 **Figure 8.** Comparison between estimated uncertainties of the 388 nm AOT (*x*-axis) and biases of
739 retrieved AOT from AERONET measurements (*y*-axis). The panels (a) and (b) are based on the
740 operational and OE-based retrieval/error-estimation algorithm, respectively.

741 **Figure 9.** Average (gray bars) and standard deviation (black lines) of the forward model parameter

errors of 388 nm (a) AOT and (b) SSA.

List of figures

[Figure 1]

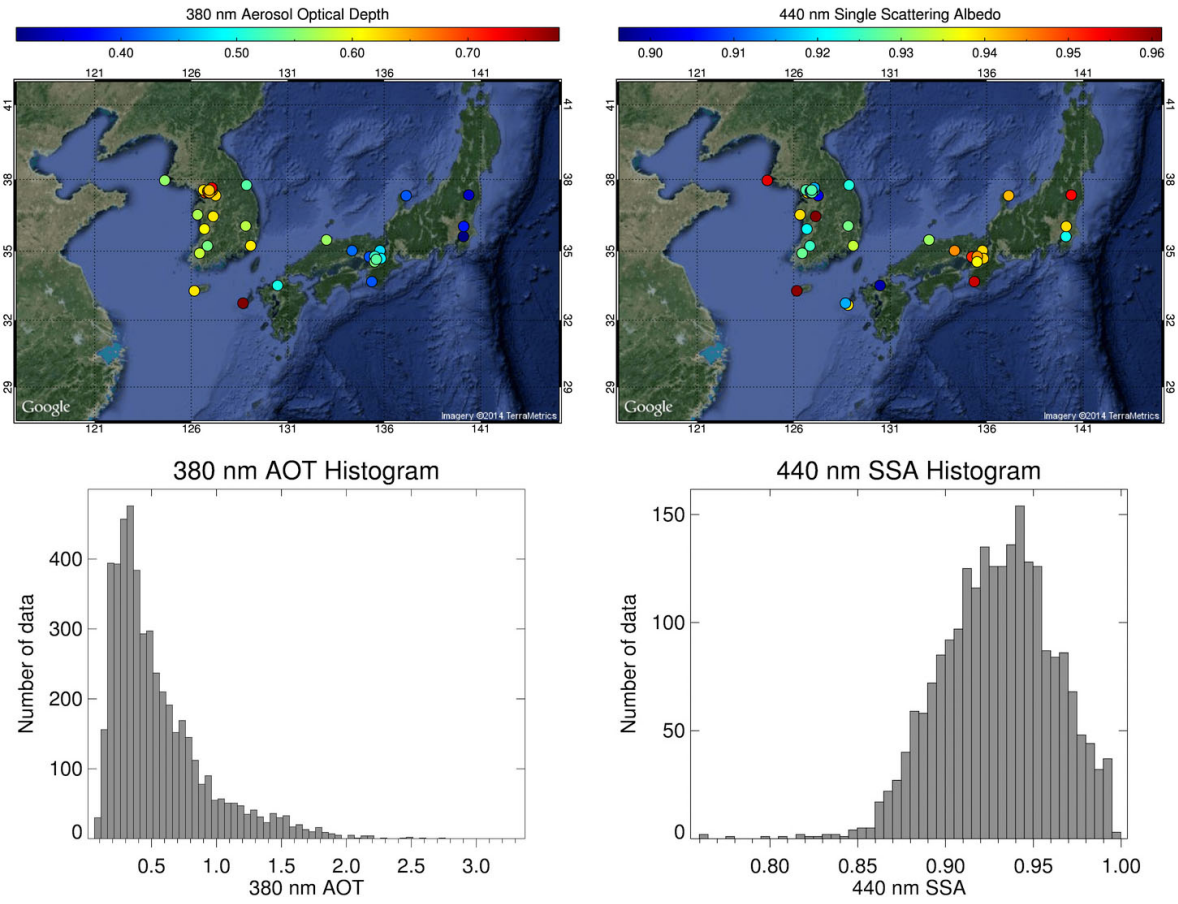

Figure 1. Mean 380 nm aerosol optical thickness (AOT) and 440 nm single scattering albedo and their probability density functions during the DRAGON-NE Asia 2012 campaign.

752 **[Figure 2]**

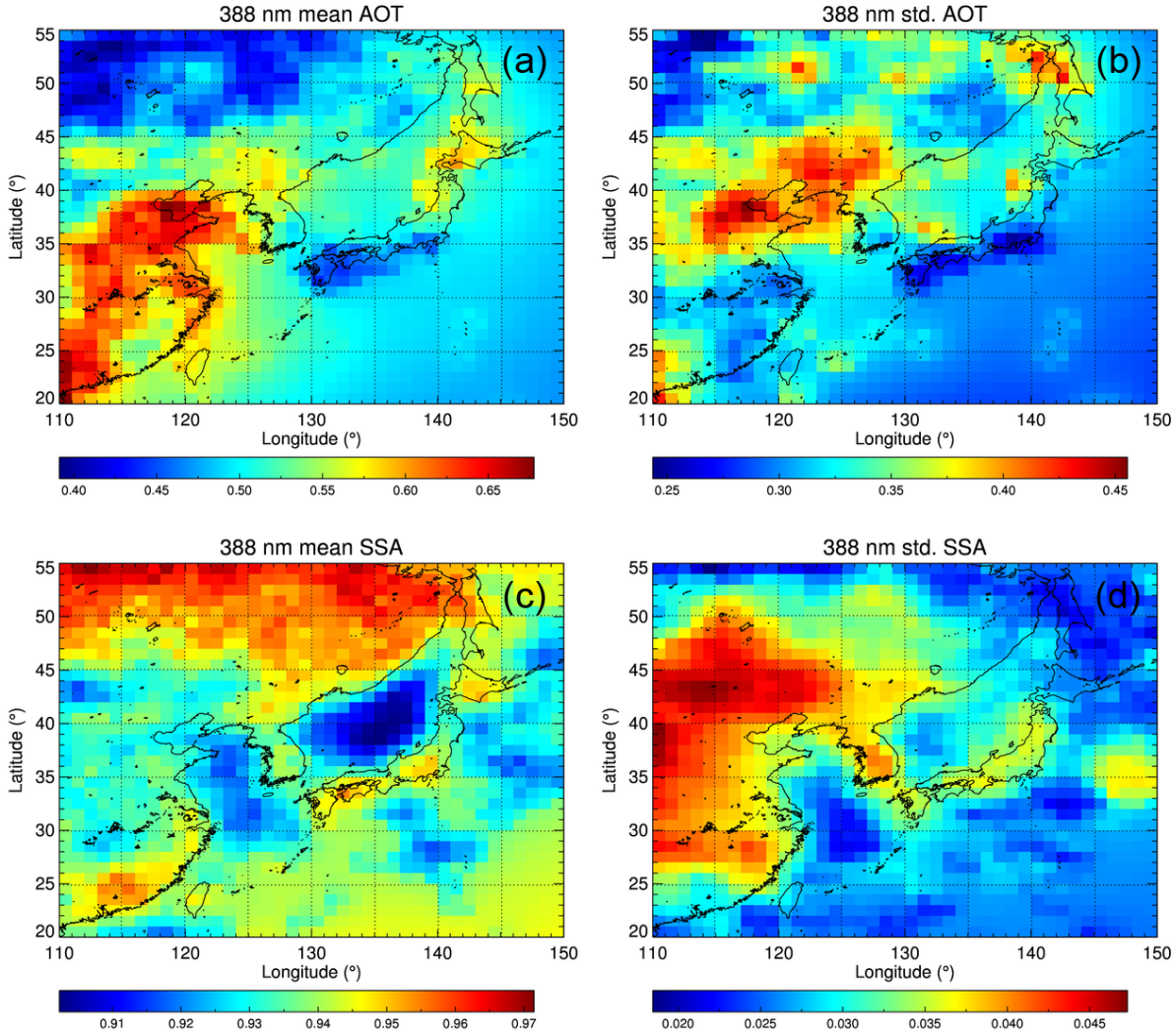

753

754 **Figure 2.** (a) Mean and (b) standard deviation of 388 nm AOT from the OMAERUV product in
755 spring (March to May) 2005–2014. Panels (c) and (d) show the average and standard deviation of
756 SSA, respectively, during the same period.

757

758 **[Figure 3]**

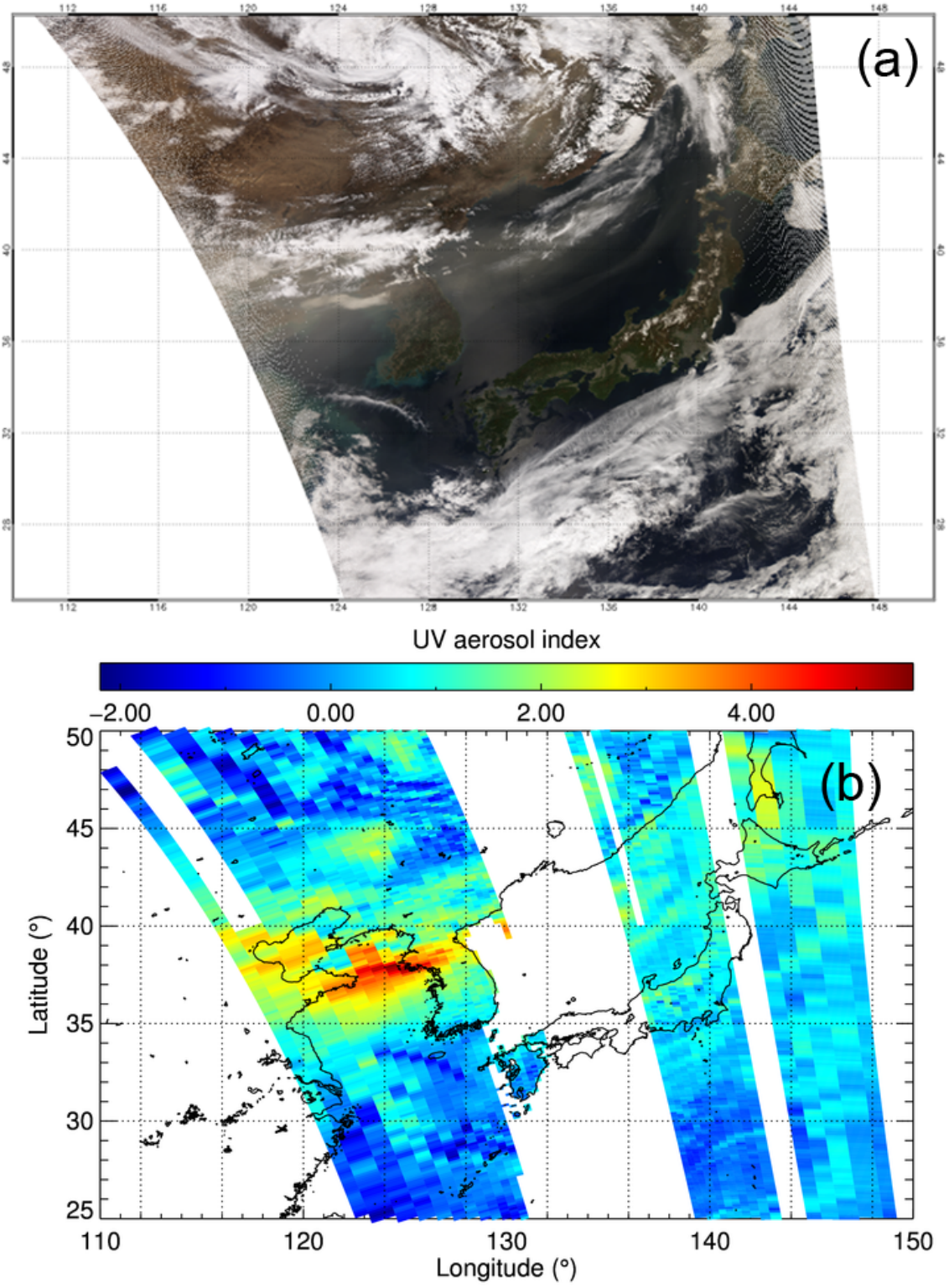

759

760 **Figure 3.** (a) MODIS Aqua true color image and (b) UV aerosol index from the OMI product in

761 Northeast Asia on 28th April 2012.

762 **[Figure 4]**

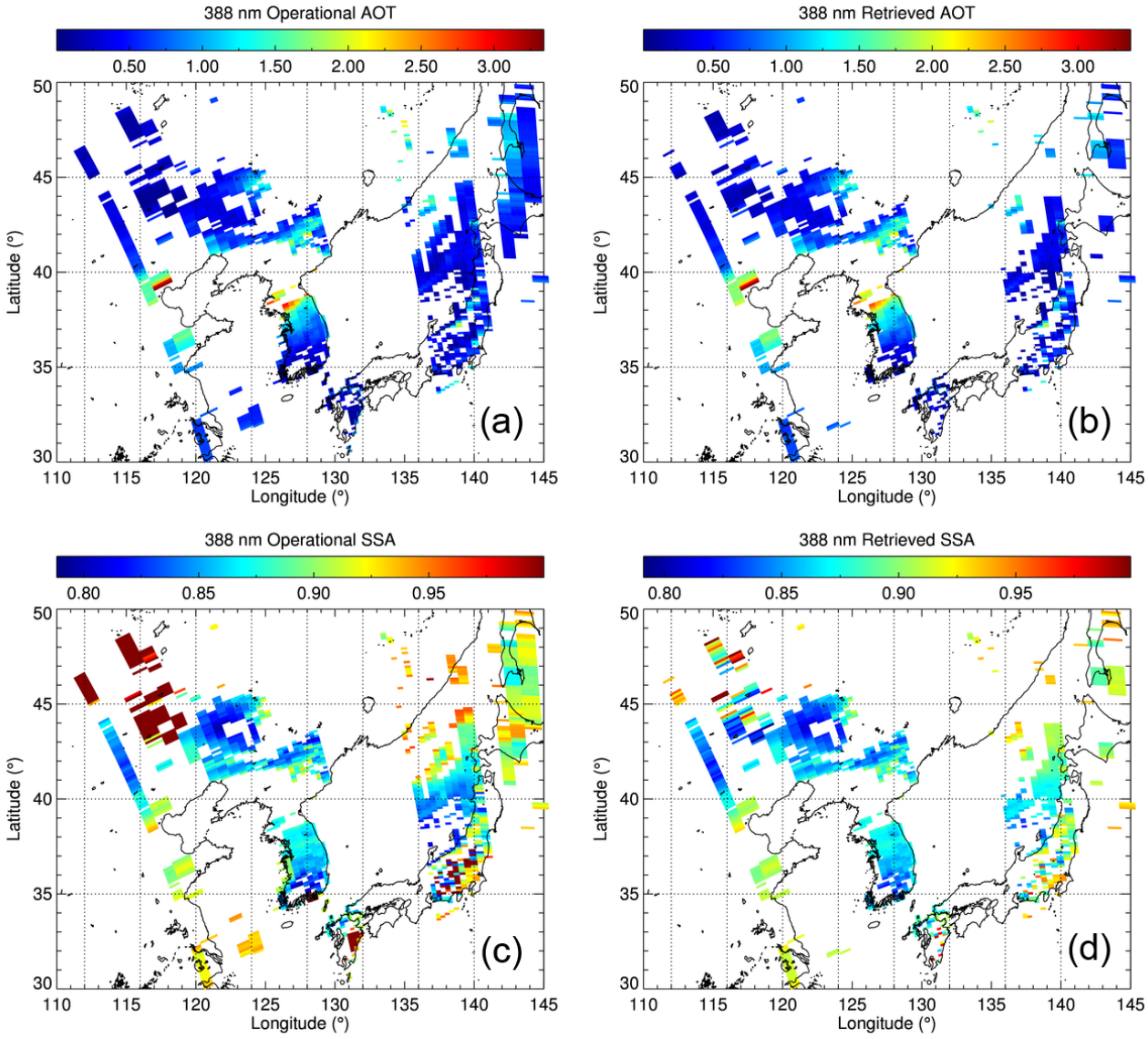

763

764 **Figure 4.** (a) OMI operational AOT, (b) OE-based AOT, (c) operational SSA, and (d) OE-based

765 SSA on 28th April 2012 at 388 nm.

766 **[Figure 5]**

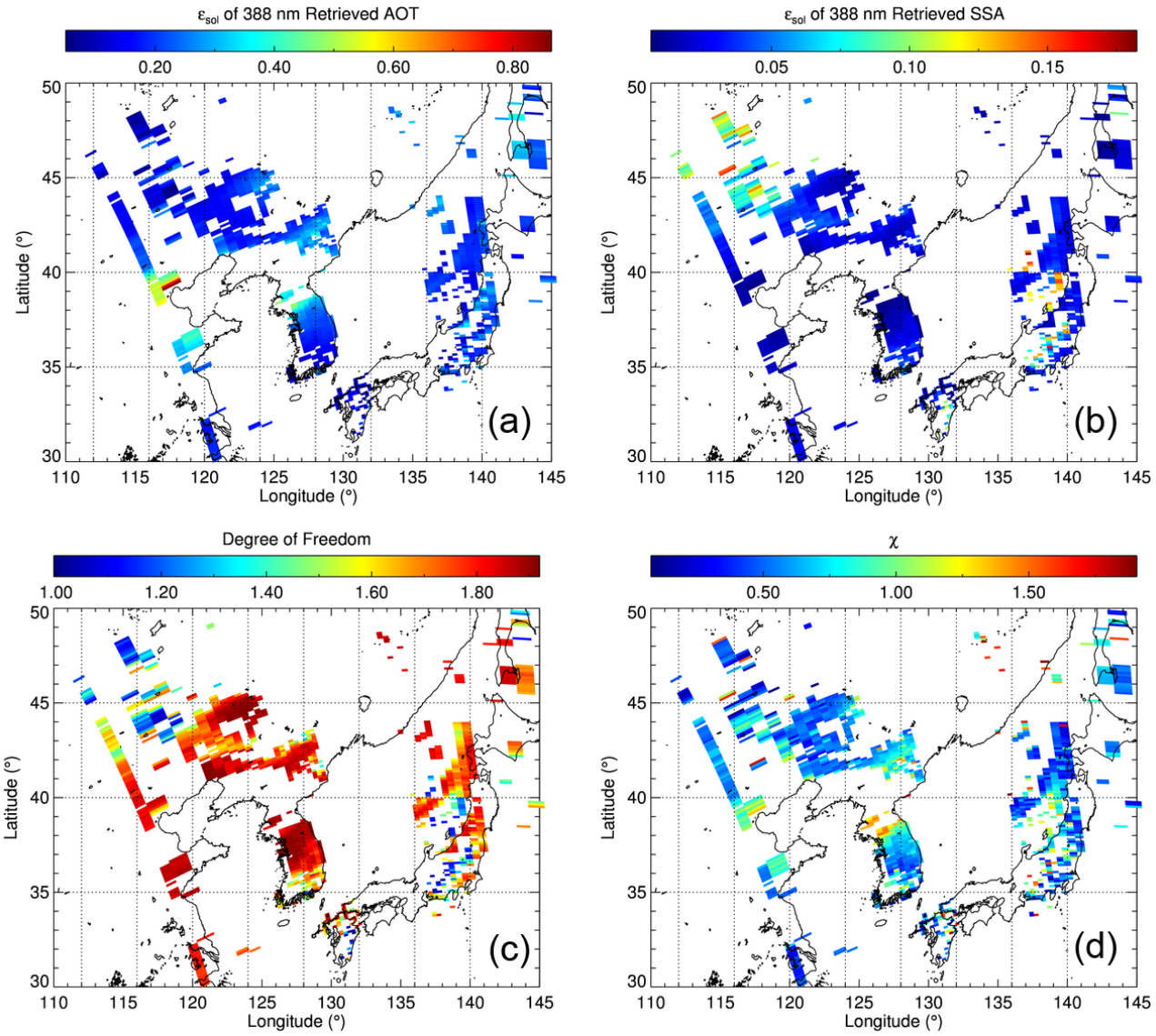

767

768 **Figure 5.** Estimated solution error of (a) OE-based 388 nm AOT and (b) SSA. Panels (c) and (d)

769 show the degrees of freedom and cost function of the retrieval, respectively.

770

771 **[Figure 6]**

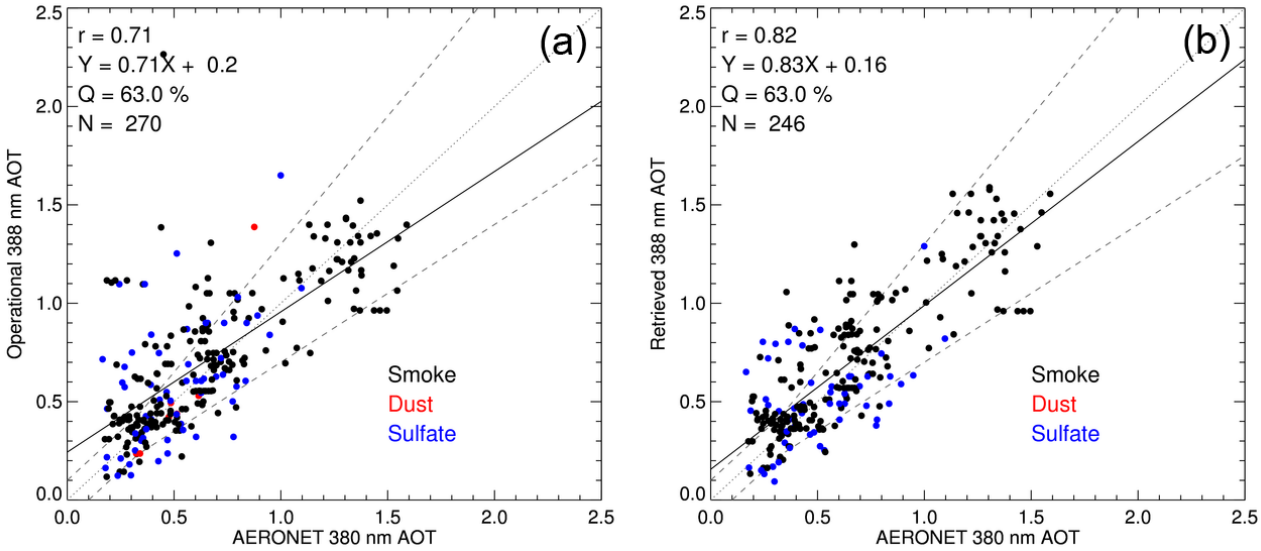

772

773 **Figure 6.** Validation of 388 nm AOT against AERONET data from (a) operational products and (b)

774 the OE-based algorithm during the DRAGON-NE Asia 2012 campaign.

775

776 **[Figure 7]**

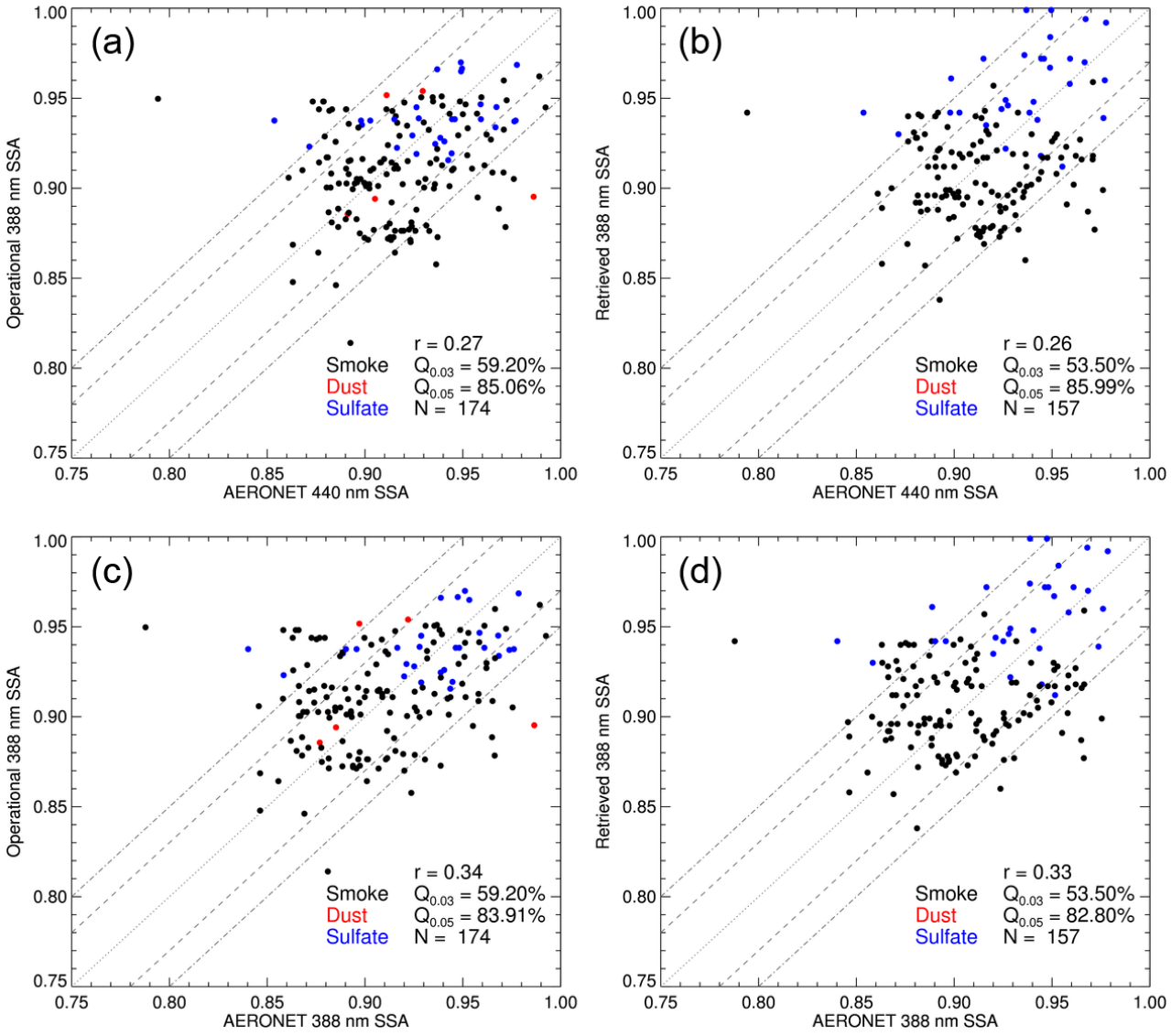

777

778 **Figure 7.** Comparison of the 440 nm SSA from AERONET and 388 nm SSA from (a) the
779 operational products and (b) the OE-based algorithm, during the DRAGON-NE Asia 2012
780 campaign. Panels (c) and (d) compare converted 388 nm SSA from AERONET with that from (c)
781 the operational products and (d) the OE-based algorithm.

782

783 **[Figure 8]**

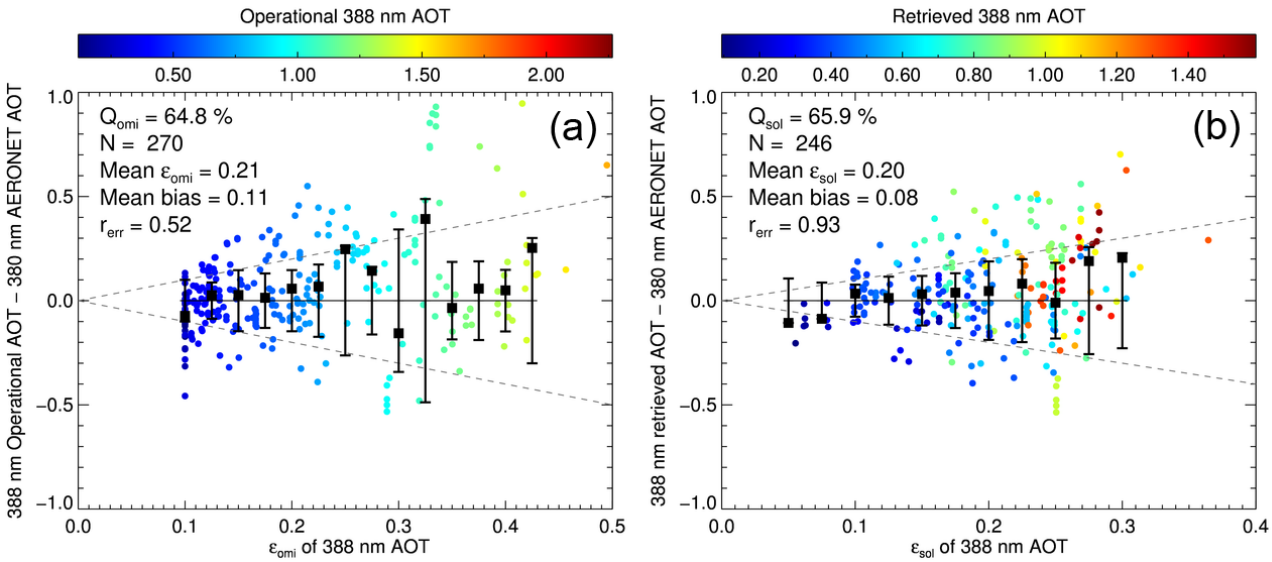

784

785 **Figure 8.** Comparison between estimated uncertainties of the 388 nm AOT (*x*-axis) and biases of
786 retrieved AOT from AERONET measurements (*y*-axis). The panels (a) and (b) are based on the
787 operational and OE-based retrieval/error-estimation algorithm, respectively.

788

789 **[Figure 9]**

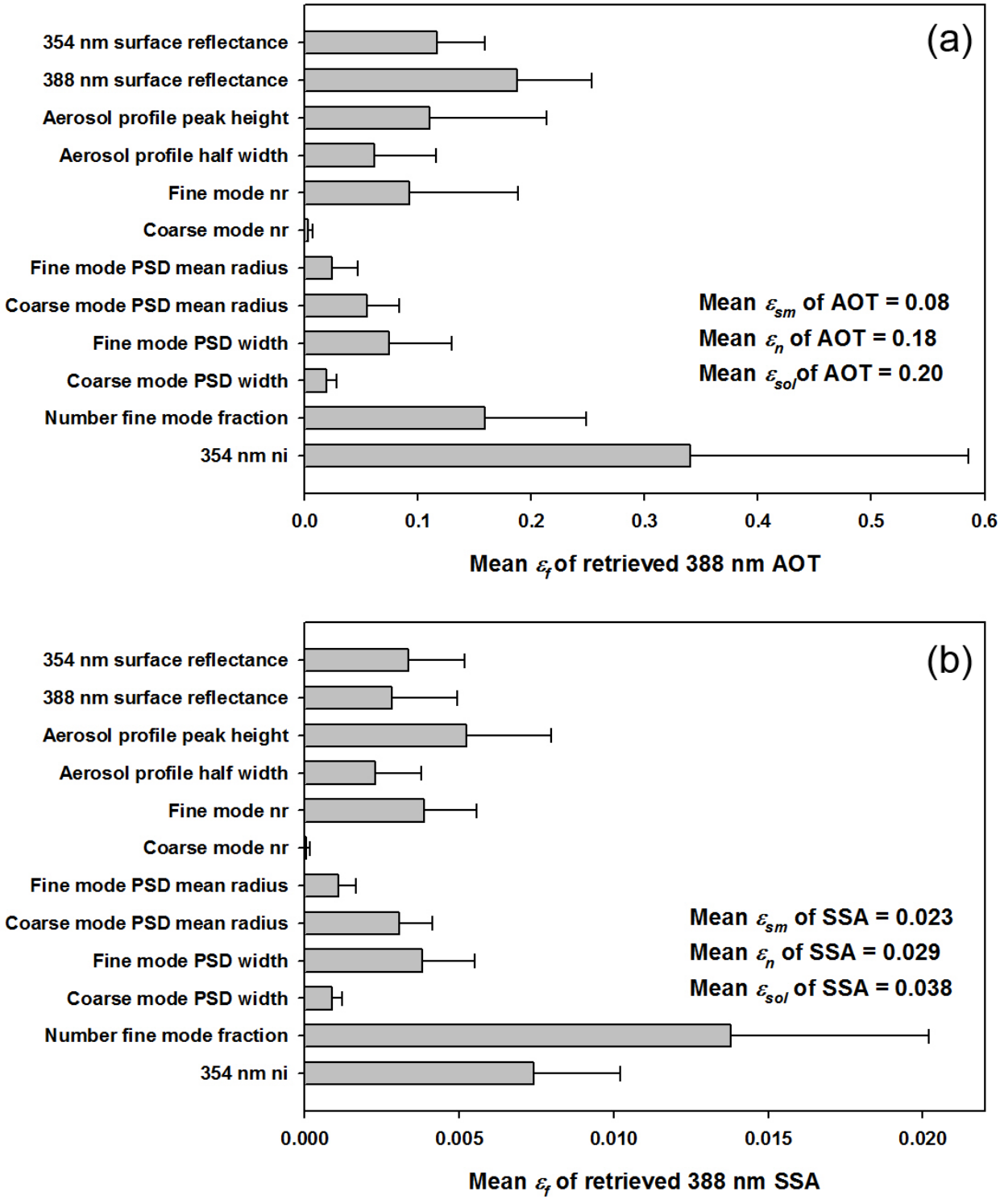

790

791 **Figure 9.** Average (gray bars) and standard deviation (black lines) of the forward model parameter

792 errors of 388 nm (a) AOT and (b) SSA.

793